
Theses and Dissertations

Spring 2011

Development of a high-resolution 1D/2D coupled flood simulation of Charles City, Iowa

Matthew Roger Moore
University of Iowa

Copyright 2011 Matthew Moore

This dissertation is available at Iowa Research Online: <http://ir.uiowa.edu/etd/1032>

Recommended Citation

Moore, Matthew Roger. "Development of a high-resolution 1D/2D coupled flood simulation of Charles City, Iowa." MS (Master of Science) thesis, University of Iowa, 2011.
<http://ir.uiowa.edu/etd/1032>.



DEVELOPMENT OF A HIGH-RESOLUTION 1D/2D COUPLED FLOOD
SIMULATION OF CHARLES CITY, IOWA

by
Matthew Roger Moore

A thesis submitted in partial fulfillment
of the requirements for the Master of
Science degree in Civil and Environmental Engineering
in the Graduate College of
The University of Iowa

May 2011

Thesis Supervisors: Professor Larry J. Weber
Adjunct Associate Professor Nathan C. Young

Graduate College
The University of Iowa
Iowa City, Iowa

CERTIFICATE OF APPROVAL

MASTER'S THESIS

This is to certify that the Master's thesis of

Matthew Roger Moore

has been approved by the Examining Committee
for the thesis requirement for the Master of Science
degree in Civil and Environmental Engineering at the May 2011 graduation.

Thesis Committee: _____
Larry J. Weber, Thesis Supervisor

Nathan C. Young, Thesis Supervisor

Witold F. Krajewski

ACKNOWLEDGMENTS

I could not have completed my research without the help of numerous people. Drs. Larry Weber and Nathan Young provided invaluable guidance in the preparation of this thesis. I want to thank Jesse Piotrowski for providing constant advice on developing my models and presenting the results. Nate, Jesse, and Andy Craig collected the bathymetric data I used in my model. Dan Gilles provided substantial help as we learned the software together. I want to thank the faculty, staff, and students at IIHR – Hydroscience and Engineering and the Iowa Flood Center for their support and friendship. Brian Miller and Mark Wilson provided support for my many computer needs. I would also like to thank Dr. Witek Krajewski for finding time in his hectic schedule to be on my thesis committee. Lastly I want to thank my parents, without their motivation, support, and positive example I would not have made it this far in my education.

ABSTRACT

The development of a high-resolution coupled one-dimensional/two-dimensional hydrodynamic model of Charles City, Iowa is presented in this study as part of a larger Iowa Flood Center initiative to create a library of steady inundation maps for communities in Iowa which have a high risk of flooding. Channel geometry from bathymetric surveys and surface topography from LiDAR were combined to create the digital elevation model (DEM) used in numerical simulations. Coupled one- and two-dimensional models were used to simulate flood events; the river channel and structures were modeled one-dimensionally, and the floodplain was modeled two-dimensionally. Spatially distributed roughness parameters were estimated using the 2001 National Land Cover Dataset. Simulations were performed at a number of mesh resolutions, and the results were used to investigate the effectiveness of re-sampling simulation results using higher- resolution DEMs. The effect of removing buildings from the computational mesh was also investigated. During 2011, the stream channel geometry is being changed as part of a recreational park in downtown Charles City. After incorporating the planned changes to the stream channel, the model was used to create a library of steady inundation maps which are available on the Iowa Flood Center website.

TABLE OF CONTENTS

| | |
|--|-----|
| LIST OF TABLES | vi |
| LIST OF FIGURES | vii |
| CHAPTER 1: INTRODUCTION | 1 |
| CHAPTER 2: LITERATURE REVIEW | 3 |
| 2.1 Hydraulic Model Background | 3 |
| 2.2 One-Dimensional Flow Models..... | 5 |
| 2.3 Two-Dimensional Flow Models..... | 6 |
| 2.4 1-D/2-D Coupled Flow Models..... | 7 |
| 2.5 Mesh Density | 8 |
| 2.6 Sources of Error | 9 |
| 2.7 Calibration of models | 10 |
| 2.8 Summary | 11 |
| CHAPTER 3: DATA COLLECTION | 15 |
| 3.1 Study Area | 15 |
| 3.2 Overview..... | 16 |
| 3.3 Bathymetry Collection..... | 16 |
| 3.3.1 Single-Beam Survey | 16 |
| 3.3.2 Survey on foot | 17 |
| 3.3.3 Contours provided by VJ Engineering | 18 |
| 3.4 In-Channel Structures | 18 |
| 3.5 Topography..... | 19 |
| 3.6 Development of Digital Elevation Model..... | 19 |
| 3.6.1 Inclusion of Bathymetry | 19 |
| 3.6.2 Inclusion of Buildings | 20 |
| 3.7 Surface Roughness..... | 20 |
| 3.8 Summary | 21 |
| CHAPTER 4: NUMERICAL SIMULATION..... | 32 |
| 4.1 Numerical Methods | 32 |
| 4.2 Boundary Conditions | 33 |
| 4.3 Structures | 34 |
| 4.4 Calibration | 35 |
| 4.5 Sensitivity Analyses..... | 35 |
| 4.5.1 Eddy Viscosity..... | 35 |
| 4.5.2 Channel Roughness | 36 |
| 4.5.3 Floodplain Surface Roughness | 36 |
| 4.5.4 Mesh Resolution | 37 |
| 4.6 Summary | 38 |
| CHAPTER 5: HIGH-RESOLUTION RE-SAMPLING RESULTS | 49 |
| 5.1 Effect of the re-sampling tool | 49 |
| 5.2 Model Application | 51 |
| 5.3 Summary | 51 |
| CHAPTER 6: SUMMARY AND RECOMMENDATIONS | 69 |
| 6.1 Summary | 69 |

| | |
|----------------------|----|
| 6.2 Future Work..... | 70 |
| BIBLIOGRAPHY | 72 |

LIST OF TABLES

| | |
|--|----|
| Table 3.1. Manning's "n" roughness based on 2001 NLCD classification..... | 31 |
| Table 4.1. Difference in water surface elevation at USGS stream gage 05457700 after model calibration..... | 40 |
| Table 4.2. Eddy viscosity sensitivity analysis results. The difference in overall water surface elevation from the results using $\epsilon = 1.67 \text{ m}^2/\text{s}$ are shown..... | 42 |
| Table 4.3. Channel roughness sensitivity analysis results. The difference in overall water surface elevation from the results using the calibrated channel roughness values are shown..... | 42 |
| Table 4.4. Floodplain roughness sensitivity analysis results. The difference in overall water surface elevation from the results using the normal roughness values are shown..... | 43 |
| Table 4.5. Fit value as compared to simulation results from the 5 m model including buildings before re-sampling..... | 44 |
| Table 5.1. Fit value as compared to simulation results from the 5 m model including buildings after re-sampling..... | 57 |
| Table 5.2. Difference in average depth from the 5 m model with buildings for each other model..... | 61 |
| Table 5.3. Computation times for each 3 day simulation in hours. Simulations were performed using dual six-core 2.67 GHz Xeon processors with 12 GB of RAM..... | 68 |

LIST OF FIGURES

| | |
|---|----|
| Figure 2.1. Example cross sections from the study reach. The cross sections in blue were extracted at 0.25 m, the resolution of the echosoundings. The cross sections in red were extracted at 5.5 m, the resolution of the survey performed on foot. Significant loss of detail occurs when extracting from a lower resolution dataset | 13 |
| Figure 2.2. Aerial view of channel bathymetry differences in a section of the study reach. Change in bed surface elevations are shown as a result of reducing resolution from 0.25 m to 5.5 m | 14 |
| Figure 3.1. The extent of the study area. The extent encompasses most of the Charles City limits. Charles City lies on both banks of the Cedar River. | 22 |
| Figure 3.2. Historic annual peak discharges at USGS stream gage 05457700 in Charles City | 23 |
| Figure 3.3. Locations and dates of bathymetric surveys..... | 24 |
| Figure 3.4. Location of structures within the study area..... | 25 |
| Figure 3.5. The process for merging bathymetry with LiDAR topography. (1) LiDAR topography. (2) The banks are converted to points and merged with channel bathymetry and used to create a TIN. (3) Elevations are extracted to cross-sections using the first TIN. A second TIN is created from extracted cross-section elevations. (4) The second TIN is converted to a raster and merged with the original topography | 26 |
| Figure 3.6. Comparison of building footprints. The figure on the left shows building footprints after re-sampling the building raster and DEM to 10 m separately and then merging. The figure on the right shows the building footprints after re-sampling a DEM with buildings already merged to 10 m..... | 27 |
| Figure 3.7. Comparison of building footprint distortion with decreasing DEM resolution | 28 |
| Figure 3.8. Distribution of 2001 National Land Cover Dataset classifications in the study area | 29 |
| Figure 3.9. Distribution of Manning's "n" roughness parameter based on 2001 NLCD classifications..... | 30 |
| Figure 4.1. 3D representation of cross-section extraction from DEM..... | 39 |
| Figure 4.2. Removal of buildings and river channel form computational mesh..... | 40 |
| Figure 4.3. Distribution of calibrated channel roughness within the study area..... | 41 |
| Figure 4.4. Fit values as compared to simulation results from the 5 m model including buildings before re-sampling. | 44 |

| | |
|---|----|
| Figure 4.5. Distribution of velocity magnitude at $Q = 1160 \text{ m}^3/\text{s}$ in downtown Charles City | 45 |
| Figure 4.6. Inundation differences from models including buildings in the downtown region of Charles City..... | 46 |
| Figure 4.7. Difference in inundation area for each model..... | 47 |
| Figure 4.8. Simulation results at a discharge of $1160 \text{ m}^3/\text{s}$ from models at 5m, 10 m, and 20 m resolutions with buildings included and removed. | 48 |
| Figure 5.1. The re-sampling process is shown. (a) Water surface elevation (WSE) result files at the original resolution. (b) The boundary of the WSE are selected and converted to points. (c) WSE is extrapolated from the boundary points using an IDW algorithm. (d) The extrapolated points are combined with the original WSE raster. DEM elevations are subtracted from the combined WSE raster. Negative depth values and disconnected areas are removed. | 53 |
| Figure 5.2. Inundation areas after and before re-sampling at a discharge of $1160 \text{ m}^3/\text{s}$. Significant increases in inundation occur after re-sampling the simulation results | 54 |
| Figure 5.3. Difference in inundation area for each simulation after re-sampling..... | 55 |
| Figure 5.4. Difference in inundation area before and after using the re-sampling tool at a discharge of $570 \text{ m}^3/\text{s}$ | 55 |
| Figure 5.5. Difference in inundation area before and after using the re-sampling tool at a discharge of $820 \text{ m}^3/\text{s}$ | 56 |
| Figure 5.6. Difference in inundation area before and after using the re-sampling tool at a discharge of $920 \text{ m}^3/\text{s}$ | 56 |
| Figure 5.7. Difference in inundation area before and after using the re-sampling tool at a discharge of $1160 \text{ m}^3/\text{s}$ | 57 |
| Figure 5.8. Cross-section of topography and water surface elevation..... | 58 |
| Figure 5.9. Plan view of cross-section of complex urban topography..... | 59 |
| Figure 5.10. Cross-section of complex urban topography showing elevation differences in the location of a street at 1m and 10m resolutions..... | 60 |
| Figure 5.11. Fit values as compared to simulation results from the 5 m model including buildings after re-sampling..... | 60 |
| Figure 5.12. Fit values of all simulations compared to 5 m model with buildings included..... | 61 |
| Figure 5.13. Difference in average depth from the 5 m model with buildings for each other model..... | 62 |

| | |
|--|----|
| Figure 5.14. Scatter plot of depth comparing the 5 m model without buildings to the 5 m model with buildings. | 63 |
| Figure 5.15. Scatter plot of depth comparing results from the 10 and 20 m models both with and without buildings at a discharge of 570 m ³ /s. | 64 |
| Figure 5.16. Scatter plot of depth comparing results from the 10 and 20 m models both with and without buildings at a discharge of 820 m ³ /s. | 65 |
| Figure 5.17. Scatter plot of depth comparing results from the 10 and 20 m models both with and without buildings at a discharge of 920 m ³ /s. | 66 |
| Figure 5.18. Scatter plot of depth comparing results from the 10 and 20 m models both with and without buildings at a discharge of 1160 m ³ /s. | 67 |
| Figure 5.19. An example of the Iowa Flood Center user interface. Users can select inundation area by predicted stage to make decisions about possible risk. | 68 |

CHAPTER 1: INTRODUCTION

In June of 2008, saturated soil and a series of heavy rainfall events led to significant flooding throughout Iowa. Millions of dollars of damage occurred, and many Iowa residents lost homes and businesses. The severity of the damage caused by the flood led to an effort to improve flood preparedness in the State. Libraries of steady flow inundations maps are being produced by the Iowa Flood Center (IFC) for a number of communities which suffered damage from the flood. One of these communities was Charles City, in northern Iowa on the Cedar River. Several homes and businesses were damaged by flood waters, and a historic suspension bridge collapsed.

A high-resolution coupled one-dimensional/ two-dimensional (1D/2D) hydrodynamic model of Charles City was developed. To develop the model, channel geometry was obtained from bathymetric surveys performed by IIHR – Hydroscience & Engineering and combined with surface topography obtained from Light Detection and Ranging (LiDAR) surveys. Roughness parameters were estimated using land use data from the 2001 National Land Cover Dataset. MIKE FLOOD coupled 1D/2D hydrodynamic modeling software was used to simulate flow. The model was calibrated using measured water surface elevations and the rating curve at the United States Geological Survey (USGS) stream gage 05457700 in downtown Charles City.

This study has two major objectives. The first objective of this study was to create a library of steady flow inundation maps. After calibration, the model was modified to incorporate planned changes in the stream channel for a kayaking park in downtown Charles City. Simulations were then performed using discharges corresponding to half-foot stage intervals at USGS stream gage 05457700. Inundation maps generated from simulation results are intended for use with National Weather Service flood forecasts, which are published as stages at USGS stream gages. Maps were also created corresponding to 10, 25, 50, 100, and 500 year return period floods. The

maps help users to identify areas at risk of inundation from the associated stage or recurrence level. Model boundary conditions were defined by official USGS flow rates (Eash, 2001). These maps can be used by residents and planners in Charles City to help make informed decisions about potential risk from floods. The maps are presented in a Google Maps format for ease of use. To facilitate widespread access to the maps, a mobile version of the IFC website is being developed.

The second objective of this study was to use the calibrated model to evaluate the effectiveness of re-sampling the simulation results using a high-resolution digital elevation models (DEMs). The re-sampling tool is designed to increase the spatial resolution of simulation results generated using coarse 2D grids. Reducing grid resolution has the benefit of reducing computation time. The re-sampling tool creates high-resolution results without increasing computation time.

CHAPTER 2: LITERATURE REVIEW

Flow of water in the natural environment can be approximated using numerical methods. The governing equations fluid flow are developed using continuity and the equations of motion. The resulting relationships, known as the Navier-Stokes equations, can be applied in three dimensions to solve complex fluid flows. Simplified one-dimensional and two-dimensional relationships, known as the St. Venant equations, are applied where a more complex description of flow is not necessary. Due to computational limitations, hydraulic models have typically solved the 1D St. Venant equations, which are computationally efficient, but cannot accurately model complex topography. Recent advances in computational capacity have made 2D solvers more feasible. A 2D model can accurately model complex topography, but is not as computationally efficient as a 1D model, and has difficulty modeling in-channel structures. Advantages of both types of models can be combined by coupling 1D and 2D models.

When developing a hydraulic model, uncertainty must be accounted for. Uncertainty in a hydraulic model can come from a number of sources. Errors in data collection can come from instrument error, resolution of collected data, and collection methods. Further uncertainty in simulation results can arise from assumptions made during model development, such as the choice of mesh resolution, methods of modeling structures, and methods of calibration.

2.1 Hydraulic Model Background

Numerical hydraulic models simulate fluid motion by solving the continuity and the Navier-Stokes equations. Continuity is described by Equation 2.1.

$$\frac{\partial \rho}{\partial t} + \frac{\partial u}{\partial x} + \frac{\partial v}{\partial y} + \frac{\partial w}{\partial z} = 0 \quad (2.1)$$

Where ρ is the fluid density, x , y , and z are Cartesian coordinates, and u , v , and w are the components of velocity in the x , y , and z directions, respectively. The equations of motion (Equations 2.2 to 2.4) are used to derive the Navier-Stokes Equations.

$$\rho g_x + \frac{\partial \sigma_{xx}}{\partial x} + \frac{\partial \tau_{yx}}{\partial y} + \frac{\partial \tau_{zx}}{\partial z} = \rho \left(\frac{\partial u}{\partial t} + u \frac{\partial u}{\partial x} + v \frac{\partial u}{\partial y} + w \frac{\partial u}{\partial z} \right) \quad (2.2)$$

$$\rho g_y + \frac{\partial \tau_{xy}}{\partial x} + \frac{\partial \sigma_{yy}}{\partial y} + \frac{\partial \tau_{zy}}{\partial z} = \rho \left(\frac{\partial v}{\partial t} + u \frac{\partial v}{\partial x} + v \frac{\partial v}{\partial y} + w \frac{\partial v}{\partial z} \right) \quad (2.3)$$

$$\rho g_z + \frac{\partial \tau_{xz}}{\partial x} + \frac{\partial \tau_{yz}}{\partial y} + \frac{\partial \sigma_{zz}}{\partial z} = \rho \left(\frac{\partial w}{\partial t} + u \frac{\partial w}{\partial x} + v \frac{\partial w}{\partial y} + w \frac{\partial w}{\partial z} \right) \quad (2.4)$$

Where σ and τ are the normal and shear stresses, respectively and g is acceleration due to gravity. Both continuity and the equations of motion hold true for any fluid at motion or at rest. For any incompressible, Newtonian fluid, stresses are linearly related to deformation rates, as shown in Equations 2.5 to 2.10.

$$\sigma_{xx} = -p + 2\mu \frac{\partial u}{\partial x} \quad (2.5)$$

$$\sigma_{yy} = -p + 2\mu \frac{\partial v}{\partial y} \quad (2.6)$$

$$\sigma_{zz} = -p + 2\mu \frac{\partial w}{\partial z} \quad (2.7)$$

$$\tau_{xy} = \tau_{yx} = \mu \left(\frac{\partial u}{\partial y} + \frac{\partial v}{\partial x} \right) \quad (2.8)$$

$$\tau_{yz} = \tau_{zy} = \mu \left(\frac{\partial v}{\partial z} + \frac{\partial w}{\partial y} \right) \quad (2.9)$$

$$\tau_{zx} = \tau_{xz} = \mu \left(\frac{\partial w}{\partial x} + \frac{\partial u}{\partial z} \right) \quad (2.10)$$

Where p is the fluid pressure is μ is the dynamic viscosity. The Navier-Stokes Equations are obtained by substituting Equations 2.5 to 2.10 into Equations 2.2 to 2.4, as shown in Equations 2.11 to 2.13.

$$\rho \left(\frac{\partial u}{\partial t} + u \frac{\partial u}{\partial x} + v \frac{\partial u}{\partial y} + w \frac{\partial u}{\partial z} \right) = -\frac{\partial p}{\partial x} + \rho g_x + \mu \left(\frac{\partial^2 u}{\partial x^2} + \frac{\partial^2 u}{\partial y^2} + \frac{\partial^2 u}{\partial z^2} \right) \quad (2.11)$$

$$\rho \left(\frac{\partial v}{\partial t} + u \frac{\partial v}{\partial x} + v \frac{\partial v}{\partial y} + w \frac{\partial v}{\partial z} \right) = -\frac{\partial p}{\partial y} + \rho g_y + \mu \left(\frac{\partial^2 v}{\partial x^2} + \frac{\partial^2 v}{\partial y^2} + \frac{\partial^2 v}{\partial z^2} \right) \quad (2.12)$$

$$\rho \left(\frac{\partial w}{\partial t} + u \frac{\partial w}{\partial x} + v \frac{\partial w}{\partial y} + w \frac{\partial w}{\partial z} \right) = - \frac{\partial p}{\partial z} + \rho g_z + \mu \left(\frac{\partial^2 w}{\partial x^2} + \frac{\partial^2 w}{\partial y^2} + \frac{\partial^2 w}{\partial z^2} \right) \quad (2.13)$$

The Navier-Stokes Equations, along with the equation of continuity, are the governing equations of motion for any incompressible, Newtonian fluid.

While the Navier-Stokes Equations provide the means to solve for fluid motion, they are typically too complex to be solved analytically. Despite the three-dimensional nature of out-of-bank flow, the preferred model will typically be the simplest (Bates and De Roo, 2000). The Navier-Stokes Equations can be simplified by depth- or section-averaging.

2.2 One-Dimensional Flow Models

The most widely adopted approach to modeling river hydraulics has been one-dimensional finite difference solution of the full St. Venant equations (Bates and De Roo, 2000). The St. Venant equations, shown in Equations 2.14 and 2.15, express both continuity and the 1D section-averaged Navier-Stokes Equation.

$$\frac{\partial A}{\partial t} + \frac{\partial Q}{\partial x} = 0 \quad (2.14)$$

$$\frac{\partial Q}{\partial t} + \frac{\partial}{\partial x} (uQ) + gA \left(\frac{\partial h}{\partial x} - S_0 \right) + gAS_f = 0 \quad (2.15)$$

Where Q is the discharge, A is the cross-sectional area, S_0 is the bed slope, and S_f is the friction slope. Basic assumptions for using the one-dimensional St. Venant Equations are that the pressure distribution is hydrostatic, the resistance relationship for unsteady flow is the same for steady flow, and the bed slope is sufficiently mild such that the cosine of the slope can be replaced by unity (Stelling and Verwey, 2005).

Widely used 1D numerical hydraulic solvers such as MIKE11 and HEC-RAS use a more general form of continuity and the section averaged Navier-Stokes Equations. The equations used in MIKE11 are shown in Equations 2.16 and 2.17.

$$\frac{\partial Q}{\partial x} + \frac{\partial A}{\partial t} = q \quad (2.16)$$

$$\frac{\partial Q}{\partial t} + \frac{\partial(\alpha Q^2/A)}{\partial x} + gA \frac{\partial h}{\partial x} + \frac{gQ|Q|}{C^2 AR} = 0 \quad (2.17)$$

Where x is the longitudinal distance, q is lateral inflow, h is flow depth, C is the Chezy coefficient, α is a momentum distribution coefficient, and R is the hydraulic radius (DHI, 2009).

While 1D models are numerically stable and computationally efficient, they may not adequately simulate lateral wave diffusion (Hunter et al., 2007) and quality of results can depend largely on the correct placement of cross-sections (Samuel, 1990). To address the shortcomings of 1D models, governing equations can be solved two-dimensionally.

2.3 Two-Dimensional Flow Models

The same principles used to derive the 1D St. Venant equations are used to derive the 2D St. Venant equations expressed in Equations 2.18 to 2.20.

$$\frac{\partial h}{\partial t} + \frac{\partial(hU)}{\partial x} + \frac{\partial(hV)}{\partial y} = 0 \quad (2.18)$$

$$\frac{\partial(hU)}{\partial t} + \frac{\partial(hUU)}{\partial x} + \frac{\partial(hVU)}{\partial y} = \frac{\partial(hT_{xx})}{\partial x} + \frac{\partial(hT_{xy})}{\partial y} - gh \frac{\partial z}{\partial x} - \frac{\tau_{hx}}{\rho} \quad (2.19)$$

$$\frac{\partial(hV)}{\partial t} + \frac{\partial(hUV)}{\partial x} + \frac{\partial(hVV)}{\partial y} = \frac{\partial(hT_{xy})}{\partial x} + \frac{\partial(hT_{yy})}{\partial y} - gh \frac{\partial z}{\partial y} - \frac{\tau_{hy}}{\rho} \quad (2.20)$$

Where h is the water depth, U and V are the depth-averaged velocity components in the x and y directions, respectively, T_{xx} , T_{xy} , and T_{yy} , are depth-averaged turbulent stresses, z is the water surface elevation, and τ_{hx} , τ_{hy} are the bed shear stresses due to friction.

The two-dimensional hydraulic model MIKE21 uses a slightly different formulation to solve 2D flows, as shown in Equations 2.21 to 2.23.

$$\frac{\partial \zeta}{\partial t} + \frac{\partial p}{\partial x} + \frac{\partial q}{\partial y} = \frac{\partial d}{\partial t} \quad (2.21)$$

$$\frac{\partial p}{\partial y} + \frac{\partial}{\partial x} \left(\frac{p^2}{h} \right) + \frac{\partial}{\partial y} \left(\frac{pq}{h} \right) + gh \frac{\partial \zeta}{\partial x} + \frac{gp\sqrt{p^2+q^2}}{C^2 h^2} - \frac{1}{\rho_w} \left[\frac{\partial}{\partial x} (h\tau_{xx}) + \frac{\partial}{\partial y} (h\tau_{xy}) \right] = 0 \quad (2.22)$$

$$\frac{\partial q}{\partial y} + \frac{\partial}{\partial y} \left(\frac{q^2}{h} \right) + \frac{\partial}{\partial x} \left(\frac{pq}{h} \right) + gh \frac{\partial \zeta}{\partial y} + \frac{gq\sqrt{p^2+q^2}}{C^2 h^2} - \frac{1}{\rho_w} \left[\frac{\partial}{\partial y} (h\tau_{yy}) + \frac{\partial}{\partial x} (h\tau_{xy}) \right] = 0 \quad (2.23)$$

Where ζ is the water surface elevation, d is the time-varying water depth, p and q are flux densities in the x and y directions, respectively, ρ_w is the density of water, and τ_{xx} , τ_{xy} , τ_{yy} are the components of effective shear stress (DHI, 2009).

Two-dimensional hydraulic models have a number of advantages over one-dimensional models. Cook and Merwade (2009) found that it is reasonable to assume that inundation extent can be more accurately predicted using 2D simulations, as influences of topographic and geometric features are more accurately represented. This advantage is especially apparent when modeling flood events in urban environments (Syme et al, 2004). Two-dimensional models are more appropriate where observations and predictions are spatially distributed, such as flood maps, whereas 1D models are preferable for point measurements of stage or discharge. (Horritt and Bates, 2002).

Reduced computational efficiency compared to 1D models is the primary disadvantage of 2D models. A balance has to be struck between spatial resolution and computation time (Horritt and Bates, 2001). Two-dimensional models are also limited in their ability to accurately simulate structures such as bridges and weirs (Frank et al, 2001), as they are not designed to model pressurized flows. A potential method for reducing computation time and adequately simulating structures is to simulate the stream channel, where flow is typically longitudinal, using a 1D model and only model flow in the floodplain two-dimensionally.

2.4 1-D/2-D Coupled Flow Models

Coupling one- and two-dimensional models takes advantage of the benefits of both methods. The main advantage of 1D/2D coupled models is the similarity between model behavior and physical behavior (Dhondia and Stelling, 2002). The use of pure 2D models is questionable (Verwey, 2001) due to the inability of a 2D model to accurately describe flow through hydraulic structures; while purely 1D models are unable to accurately simulate flow in complex terrains, such as urban environments (Syme, et. al,

2004). Purely 1D models are unable to model flow into the floodplain when structures such as floodwalls are present (Frank, 2001). Modeling the stream channel one-dimensionally can also allow for reducing grid cell resolution in the 2D model when the stream channel is very narrow (Dhondia and Stelling, 2002). In a purely 2D model, the grid cell size is governed by the width of the channel.

MIKE FLOOD couples the 1D MIKE11 and 2D MIKE21 software from DHI-Water & Environment. A number of options are available for linking the two models. Lateral linkage explicitly couples MIKE11 to MIKE21 by modeling water entering the floodplain from the stream channel laterally. The flow from the stream channel to the floodplain is modeled using a simple weir equation. Momentum is not conserved using lateral links, due to the inability of 1D models to simulate cross-channel flow (DHI, 2009).

2.5 Mesh Density

A number of considerations must be made to determine the appropriate mesh density used in a 2D model. As stated previously, in a purely 2D model, the minimum cell size is defined by the width of the stream channel (Dhondia and Stelling, 2002). The 2D model must be able to adequately represent the stream channel to accurately simulate flow. Using a coupled 1D/2D model avoids this requirement, as the stream channel is only modeled one-dimensionally.

When modeling urban settings, the minimum grid cell size can be estimated by the shortest length scale of urban structures (Fewtrell et al, 2008). In most cases, the shortest length scale of urban structures will be the distance between buildings. With this criterion, flood simulations of urban settings typically require a much higher resolution than flood simulations of rural settings. The mesh resolution must also be dense enough to accurately represent storage areas near the channel, as these areas can significantly reduce travel time of the flood wave (Horritt and Bates, 2001).

2.6 Sources of Error

From data collection through model development there are a number of sources of error which must be taken into consideration. Propagation of errors in model development may lead to inaccurate or misleading results.

In the data collection stage, uncertainties in instrumentation must be considered. The methods used to obtain data can also introduce errors. For the region investigated in this study, bathymetric data was collected using different methods. The majority of the reach was surveyed using a single-beam echosounder. A portion of the bathymetry was collected with a Global Positioning System (GPS) receiver by traversing transects of the stream channel on foot. The average distance between data points collected by the echosounder was 0.25 m. The average distance between data points collected on foot was 5.5 m. Due to the computational efficiency of 1D models, it is preferred to extract cross-sectional geometry at high-resolutions. Figure 2.1 shows some examples of the differences in cross-sectional geometry when extracting from both high and low-resolution Digital Elevation Models (DEM). Figure 2.2 shows the differences in bed surface elevations extracted from a high-resolution DEM and a low-resolution DEM. Cook and Merwade (2009) found that inundation area decreased by up to 25% in a HEC-RAS model when increasing resolution from 30 m to 6 m. Using a 2D model, Fewtrell et al (2008) found that deriving a coarse-resolution mesh from a fine-resolution mesh produced approximately 20% difference in inundation extents and ± 0.1 m difference in water surface elevation.

Roughness parameters can have a large effect on model results. Models are typically calibrated by adjusting roughness to produce results which closely reproduce observed data. As flood models are non-linear, optimal roughness parameters are likely to differ over a range of discharges (Romanowicz and Beven, 2003; Bates et al, 2004). A Monte Carlo uncertainty analysis can be performed to determine the uncertainty associated with the parameters.

Other parameters which are often neglected may also have an effect on the accuracy of model results. Sauer and Meyer (1992) found that few studies investigating the effect of boundary effects, ice, flow obstructions, or wind on calculation results have been performed. The importance of flow obstructions is particularly relevant to flood simulations. Trees and other debris often collect at structures in the stream channel and can alter the water surface elevation.

2.7 Calibration of models

Models are typically calibrated using previously observed data. A number of parameters can be adjusted within accepted ranges to produce desired results. The traditional method of calibrating models is to reduce the difference between observed and predicted values (Aronica et al, 1998) by adjusting distributed parameters. Parameters which can be adjusted to produce a calibrated model are surface roughness in the channel or floodplain, eddy viscosity, and mesh resolution. The dominating parameter for a 1D model is typically channel roughness (Hall, 2005). Two-dimensional models are relatively insensitive to changes in floodplain roughness (Pappenberger, 2006) and changes in mesh density (Horritt and Bates, 2001), so in a coupled 1D/2D model, the dominating parameter should be the channel roughness. Structures within the channel also must be accurately modeled as their presence can have a large effect on model results (Pappenberger, 2007).

Adjusting parameters to reproduce observed data is somewhat problematic and exposes shortcomings inherent in the model. Romanowicz and Beven (2003) found that the calibrated distribution of channel and floodplain roughness can vary depending on the magnitude of flow being modeled. The same results were found by Bates et al (2004) when using a Monte Carlo analysis of parameter uncertainty. For such complex distributed models it may be beneficial to use a statistical calibration of model parameters, as observation errors and modeling errors will always exist (Aronica et al,

1998). Furthermore, a global calibration of models may lead to subpar performance in local areas, so it can potentially be beneficial to calibrate a model to a localized area of high importance, rather than globally calibrating a model (Pappenberger et al, 2007). In a mixed urban/rural setting, calibrating the model to ensure the most heavily occupied areas are most accurately simulated may be preferable.

Stream gage rating curves are often used to calibrate hydraulic models. However, using stream gages for calibration can also be problematic as rating curves are subject to error. One study found an error of 18-25% at peak flow in the investigated rating curve (Pappenberger, 2006). The method used to generate the rating curve can substantially alter results. A study performed by Domeneghetti et al. (2010) developed a rating curve by fitting to previously measured data, which was then used to calibrate the model by adjusting the Manning's "n" roughness coefficient. The rating curve was then developed using fitted data and simulated discharge capacity. After calibrating the model to the new rating curve, it was found that the Manning's "n" roughness coefficient had changed by as much as 59%.

2.8 Summary

It is possible to simulate a natural process such as fluid flow using numerical models. The governing equations used for modeling hydrodynamics are the Navier-Stokes equations and continuity. These relationships can model the complex three-dimensional flow present in flood flows. However, in most situations it is unnecessary to model flows with such complexity. Simplified one-dimensional and two-dimensional relationships, known as the St. Venant equations, are typically more appropriate for flood simulations. Both 1D and 2D models have advantages and disadvantages. Coupling the 1D and 2D models by modeling flow in the stream channel one-dimensionally and flow in the floodplain two-dimensionally creates a "best of both worlds" approach (Bishop and Catalano, 2001).

In urban settings, the appropriate mesh density used by the 2D model can be estimated by the distance between buildings. The mesh density must also be high enough to adequately represent storage areas near the channel.

There are many sources of error in model development. These errors will affect the accuracy of results produced by a model. Model parameters can be adjusted to calibrate the model to observed measurements. Calibrating a model is necessary; however, calibration can also be problematic. Errors will always be present in both observed and simulated data, and it may be beneficial to employ a statistical calibration.

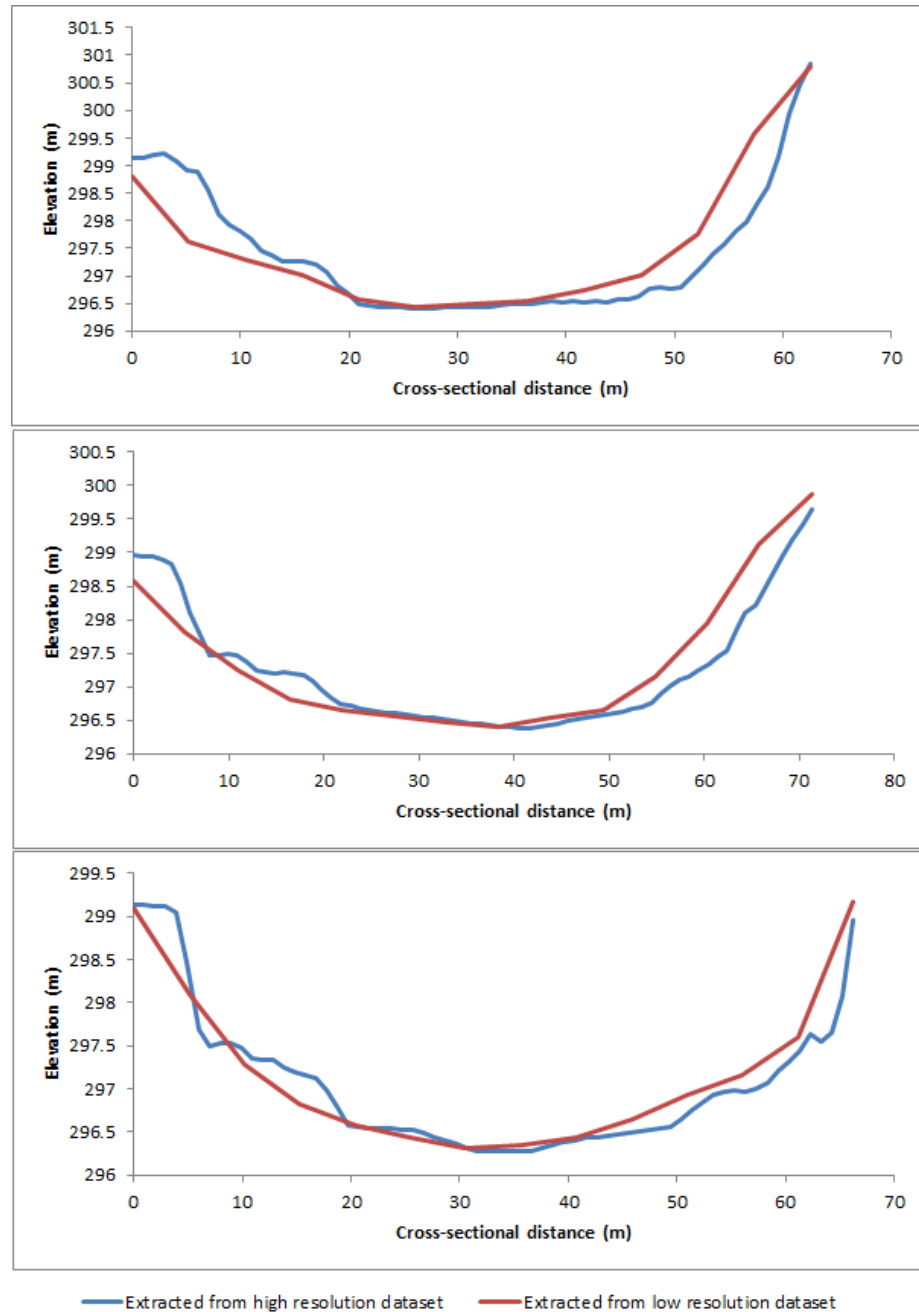


Figure 2.1. Example cross sections from the study reach. The cross sections in blue were extracted at 0.25 m, the resolution of the echosoundings. The cross sections in red were extracted at 5.5 m, the resolution of the survey performed on foot. Significant loss of detail occurs when extracting from a lower resolution dataset.

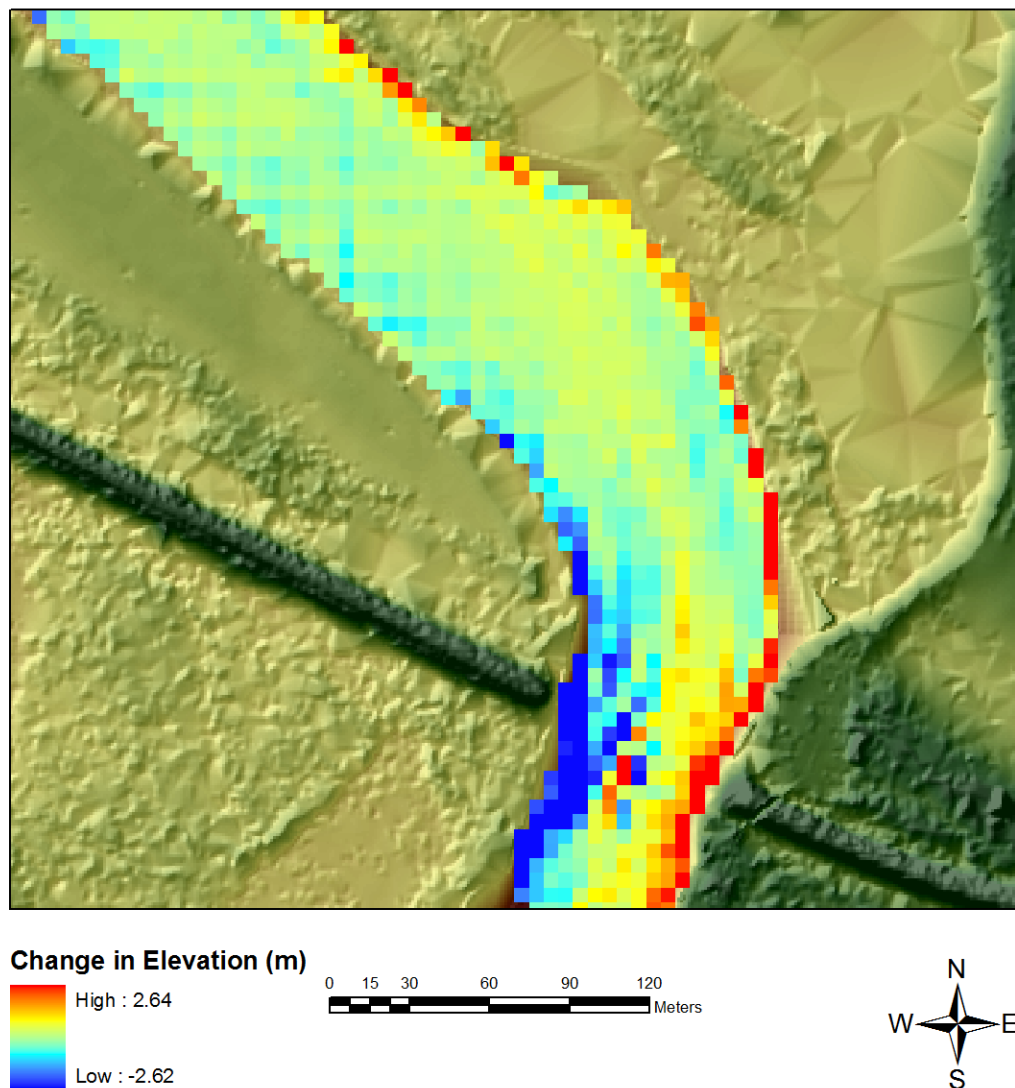


Figure 2.2. Aerial view of channel bathymetry differences in a section of the study reach. Change in bed surface elevations are shown as a result of reducing resolution from 0.25 m to 5.5 m.

CHAPTER 3: DATA COLLECTION

A number of geometric data sources were necessary to create the 1D/2D coupled hydraulic model used for simulating flood events in Charles City. A DEM served as the basis for creating 1D cross-sections and the 2D computational mesh. To create the DEM, channel bathymetry obtained from surveys was combined with surface topography derived from Light Detection and Ranging (LiDAR) surveys. Buildings were added to the surface topography and bridges and dams were added to the 1D cross-sections. Surface and channel roughness were derived from land use obtained from the 2001 National Land Cover Dataset (NLCD).

3.1 Study Area

Charles City is located in northeast Iowa along the banks of the Cedar River. The study area is shown in Figure 3.1. The river reach within the study area is approximately 12.5 km in length, running from northwest to southeast through the city limits of Charles City. The entire study area covers 48.8 square kilometers. The city itself covers 16.1 square kilometers of the study area. There are five bridges and two dams within the study reach, including a historic suspension bridge that collapsed during the 2008 flood.

United States Geological Survey (USGS) stream gage 05457700 is located 800 ft (244 m) downstream of the bridge crossing at Brantingham Street. The drainage area at the USGS gage is 2730 km². Stage and discharge have been recorded continuously at the gage since 10/1/1964. Peak discharge records extend back to 1946 and are shown in Figure 3.2. The three largest floods on record occurred in 1961, 1999, and 2008. The extreme discharge during the 2008 disabled the stream gage in downtown Charles City during the peak flow days of 6/8/2008-6/10/2008. The estimated 2008 flow rate is the largest on record for Charles City.

3.2 Overview

Creating the DEM used in the numerical simulation required integration of channel bathymetry, surface topography, and buildings within the floodplain. The majority of the channel bathymetry was collected in surveys performed by IIHR–Hydroscience & Engineering. A small portion of the channel bathymetry was obtained from a survey performed by VJ Engineering. Surface topography was obtained as 1 m resolution LiDAR from the Iowa Department of Natural Resources Geographic Information Systems Library (IDNRGIS). Building footprints were delineated using high-resolution aerial photography.

In-channel structures such as bridges and dams were added to the one-dimensional model. Plans for two of the bridges and one of the dams were provided by Charles City. As-built plans were unavailable for the rest of the structures as the Charles City hall of records was destroyed by a tornado in 1968 and the plans were lost. These remaining structures were surveyed by IIHR – Hydroscience & Engineering using GPS.

3.3 Bathymetry Collection

The survey locations and dates of each section of the study reach are shown in Figure 3.3. Bathymetry for the majority of the study reach was collected using a single-beam echosounder. A large section of bathymetry was collected using a GPS receiver and performing transects on foot. The remainder of the bathymetry was supplied by VJ Engineering.

3.3.1 Single-Beam Survey

Four sections of the study reach were surveyed by IIHR – Hydroscience & Engineering using a single-beam echosounder. These surveys took place on 8/4/09, 8/5/09 and 3/24/10. These sections cover approximately 6.4 km upstream of Main Street Dam in downtown Charles City and 3.7 km downstream of the Charley Western Bike Trail Bridge (Figure 3.3).

Channel bed soundings were collected using a 200 kHz Odom Hydrographic HT100 survey-grade single-beam sonar with a 3-degree transducer. A Trimble R8 real-time kinetic (RTK) Global Navigation Satellite System (GNSS) receiver was used to geo-reference the echosoundings. The Iowa Department of Transportation (DOT) Real Time Network (IaRTN) provided horizontal and vertical RTK corrections. The depth soundings were synchronized with the geo-referenced position of the sonar head using HYPACK 2008, a hydrographic surveying software package, which also recorded the data in real time. The water surface elevation data were time averaged using a 30 second moving window. The depth was recorded with the assumption that the Trimble R8 receiver was in the exact position of the sonar head. To correct this, the depth soundings and the distance from the sonar head to the Trimble R8 receiver were subtracted from the time averaged elevation readings from the receiver. Calculating bed elevation in this way assumes the Trimble R8 receiver is directly above the sonar head and the sonar head is normal to the bed surface at all times. This assumption is often violated due to pitch, heave, and roll of the boat. Some data points were removed where inaccurate readings occurred. These inaccuracies typically occurred under tree cover at the banks, where the foliage blocked clear readings from the satellites.

HYPACK 2008 was then used to filter the data. Bed elevations with a horizontal/vertical dilution of precision greater than 0.02 m and 0.04 m, respectively, were removed. Bed elevations that varied significantly from adjacent soundings were manually removed as well. Inconsistencies in geographic readings were determined by locating soundings that were far from adjacent soundings; the inconsistent readings were then removed in ArcGIS.

3.3.2 Survey on foot

A shallow portion of the study reach, extending from Beauty Dam to the Charley Western Trail bridge, approximately 1.8 kilometers in length, was surveyed by transects

at approximately 30 m intervals on foot on 9/16/09. The bed surface elevation was obtained using a Trimble R8 RTK GNSS receiver. The IaRTN was used as the horizontal and vertical RTK corrections. Unlike the single-beam survey, the bed surface elevation was measured directly.

3.3.3 Contours provided by VJ Engineering

A section of the study reach in the vicinity of channel structures was determined to be unsafe to survey at the times that IIHR – Hydroscience & Engineering was at the location. A large portion of this particular section had been previously surveyed by VJ Engineering in preparation for a recreational development in downtown Charles City. The topography for this section was supplied by VJ Engineering as a set of 1 ft bathymetric contours. These bathymetric contours cover the section from Main Street Bridge to Brantingham Street Bridge.

3.4 In-Channel Structures

Structure locations are shown in Figure 3.4. Detailed as-built plans for Brantingham Street Bridge were supplied by the Iowa Department of Transportation (IDOT). Changes to channel bathymetry to create a recreational kayak park in downtown Charles City are ongoing, as of 5/5/2011. Details from the planned recreational park included the current geometry of Beauty Dam. Plans for the suspension bridge and the downtown kayaking park were supplied by Charles City. The suspension bridge that collapsed during the 2008 flood has been re-built, and was included in the model. The remaining structures, Main Street Dam, Main Street Bridge, Charley Western Trail Bridge, and a pedestrian bridge in downtown Charles City, were surveyed by IIHR – Hydroscience & Engineering.

None of the five bridges or two dams were included within the DEM. All of these structures were added to the one-dimensional model after the DEM was used to create the channel and floodplain geometry for the model. Since the section modeled one-

dimensionally was blocked out of the 2D computational mesh, it was not necessary to include the structures within the DEM.

3.5 Topography

Surface topography for the study area was obtained as a 1 m resolution LiDAR raster from the IDNRGIS, collected as part of an initiative to map topography for the entire state of Iowa. A bare earth LiDAR DEM, with buildings and trees removed from the topography, was used as the basis for the creation of the DEM used in the model.

3.6 Development of Digital Elevation Model

Both the 1D and 2D models were created using a DEM, incorporating channel bathymetry, buildings, and surface topography. Channel geometry for the 1D cross-sections were extracted from the model DEM. The model DEM was also used as the computational mesh in the 2D simulation after re-sampling at lower resolution.

3.6.1 Inclusion of Bathymetry

Merging the collected bathymetry with the LiDAR topography was essential for creating a computational mesh that was physically consistent with the surface of the study reach. The geometric description of the river channel and surrounding topography can greatly affect the results from a hydraulic model (Merwade et al, 2008). The process applied in this investigation is shown in Figure 3.5. First, the banklines were delineated to separate the areas of the LiDAR data which would be retained from the area where the bathymetry would be added. The bathymetry soundings were then used to create a Triangular Irregular Network (TIN). The TIN was then merged with overbank topographic data. The elevation was then extracted from the TIN at the surveyed transects and interpolated in the streamwise direction. The contours provided by VJ Engineering were then merged with the DEM. The contours extended to the banks, so no interpolation from the channel to the banks was necessary. A bounding polygon was

created surrounding the contours, which were then used to create a TIN. The TIN was converted to a raster and merged onto the DEM.

3.6.2 Inclusion of Buildings

While the inlet and outlet of the modeled reach are in rural settings, the majority of the reach runs through residential and business districts within Charles City. Buildings in areas of lower elevation where flooding could possibly occur were included within the surface topography. The building footprints were delineated in ArcGIS using aerial photography and LiDAR data. No elevation data were available for buildings, so an assumed value sufficiently high to effectively remove them from the computational mesh was used. The building polygons were then converted to a building raster at 1 m resolution. The model DEM and building raster were re-sampled to lower resolutions separately and then merged, as merging prior to re-sampling caused a loss of definition in building footprints as shown in Figure 3.6. Maintaining clearly defined building footprints allowed for the model to simulate flow between buildings. Re-sampling a DEM with buildings already included caused the buildings to merge into large structures, which could potentially block flow. Re-sampling of the buildings to lower resolutions progressively caused distortion of building geometry as shown in Figure 3.7.

3.7 Surface Roughness

Land use for the study area was obtained from the 2001 National Land Cover Dataset (NLCD), developed by a consortium of US agencies (USDA 2010). The distributed NLCD categories are shown in Figure 3.8. Each land use was assigned a Manning's "n" roughness parameter using established literature (Chow, 1959). Roughness coefficients from land uses not described by Chow were determined from Calenda (2005). Calenda did not assign a range of roughness like those provided by Chow. To determine a range, the average range of minimum and maximum values from normal of the Chow values was calculated. The calculated range of minimum and

maximum values were rounded to $\pm 25\%$ of the normal values and applied to the Calenda values. The roughness distribution in the study area is shown in Figure 3.9 and the values used are shown in Table 3.1.

3.8 Summary

Data for creating the numerical model were collected from a number of sources. Most of the Cedar River bathymetry in the Charles City area was collected by IIHR – Hydroscience & Engineering. The remaining bathymetry was provided by VJ Engineering. Topography was provided by the IDNR as high-resolution LiDAR data. Channel bathymetry was merged with topographic data to create the model DEM. This model DEM was used to create cross-sections for the 1D simulations, and as the computational mesh for the 2D simulations. Structures were incorporated in the 1D network file. Structure geometry was provided by IDOT and Charles City. Structures where plans were not available were surveyed by IIHR – Hydroscience & Engineering. Land use was used for estimating surface roughness. Land use was provided as the 2001 National land Cover Dataset. All of these elements were necessary to create the numerical model of flooding in Charles City.

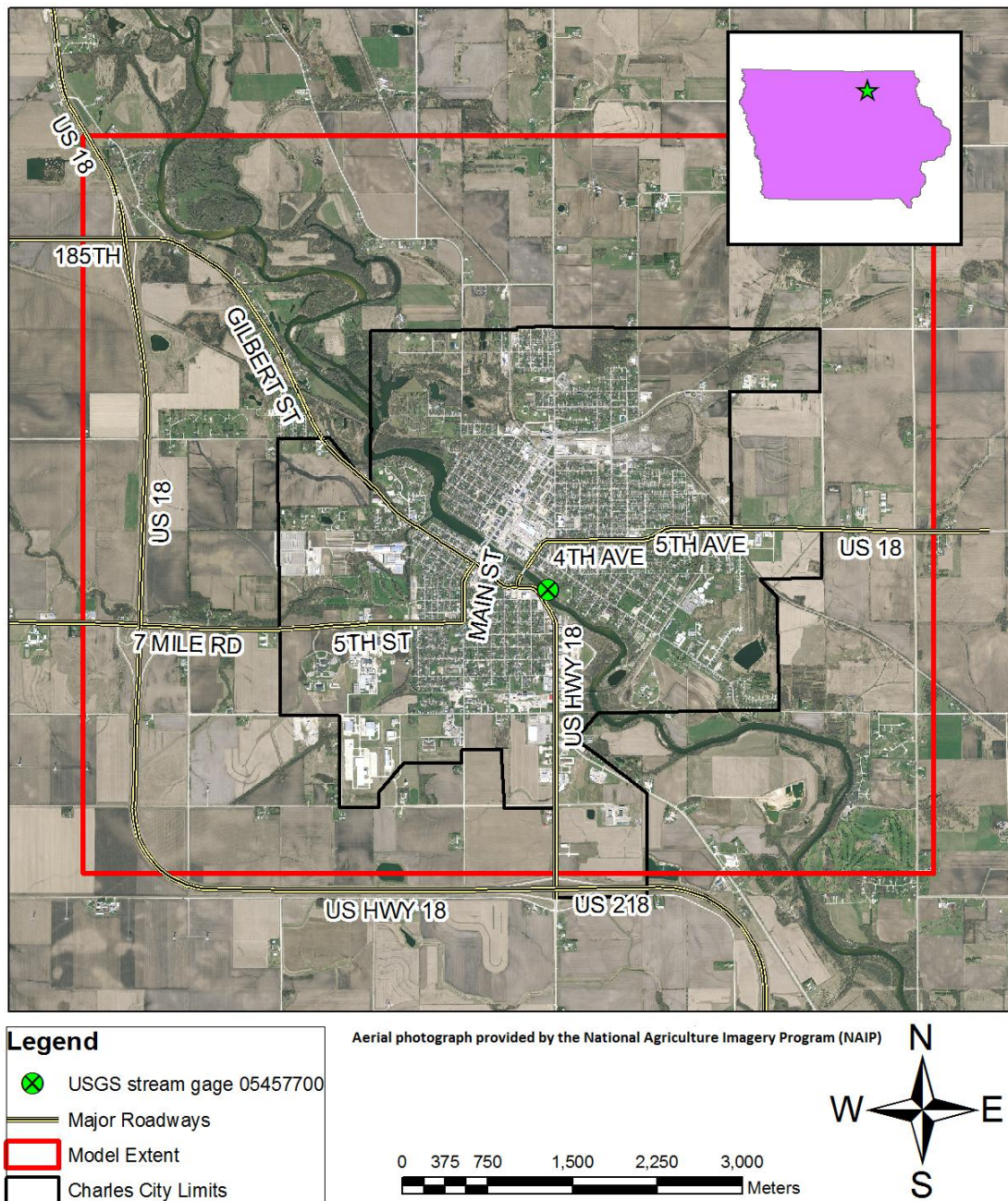


Figure 3.1. The extent of the study area. The extent encompasses most of the Charles City limits. Charles City lies on both banks of the Cedar River.

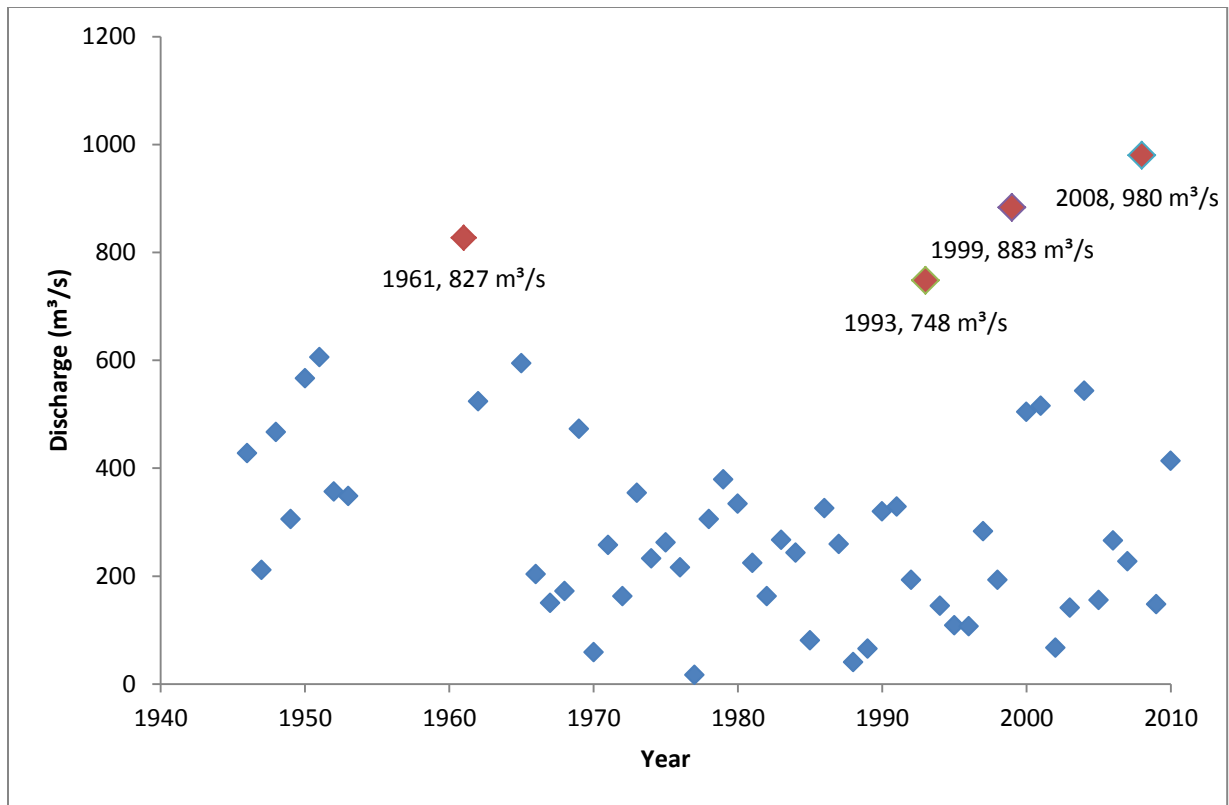


Figure 3.2. Historic annual peak discharges at USGS stream gage 05457700 in Charles City.

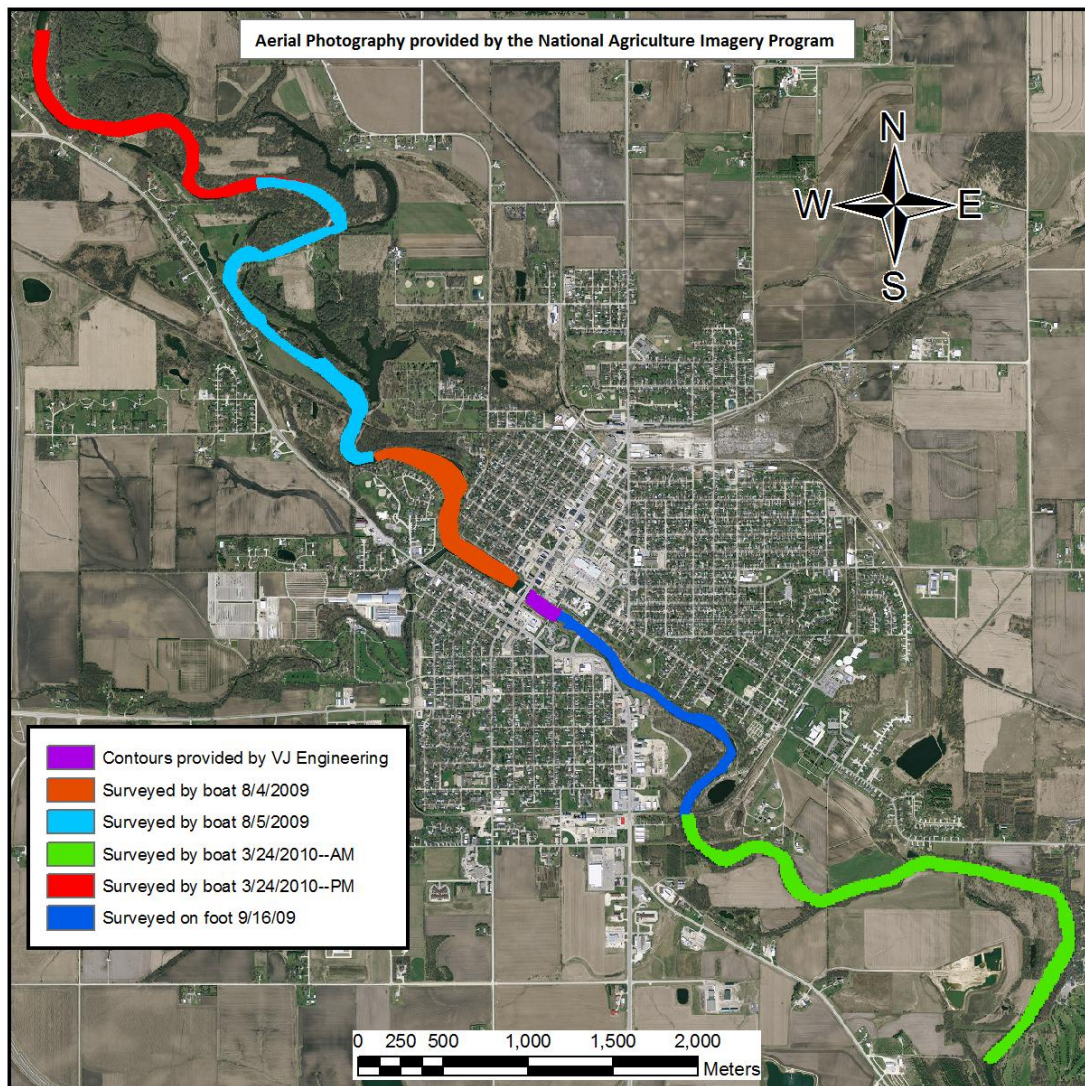


Figure 3.3. Locations and dates of bathymetric surveys.

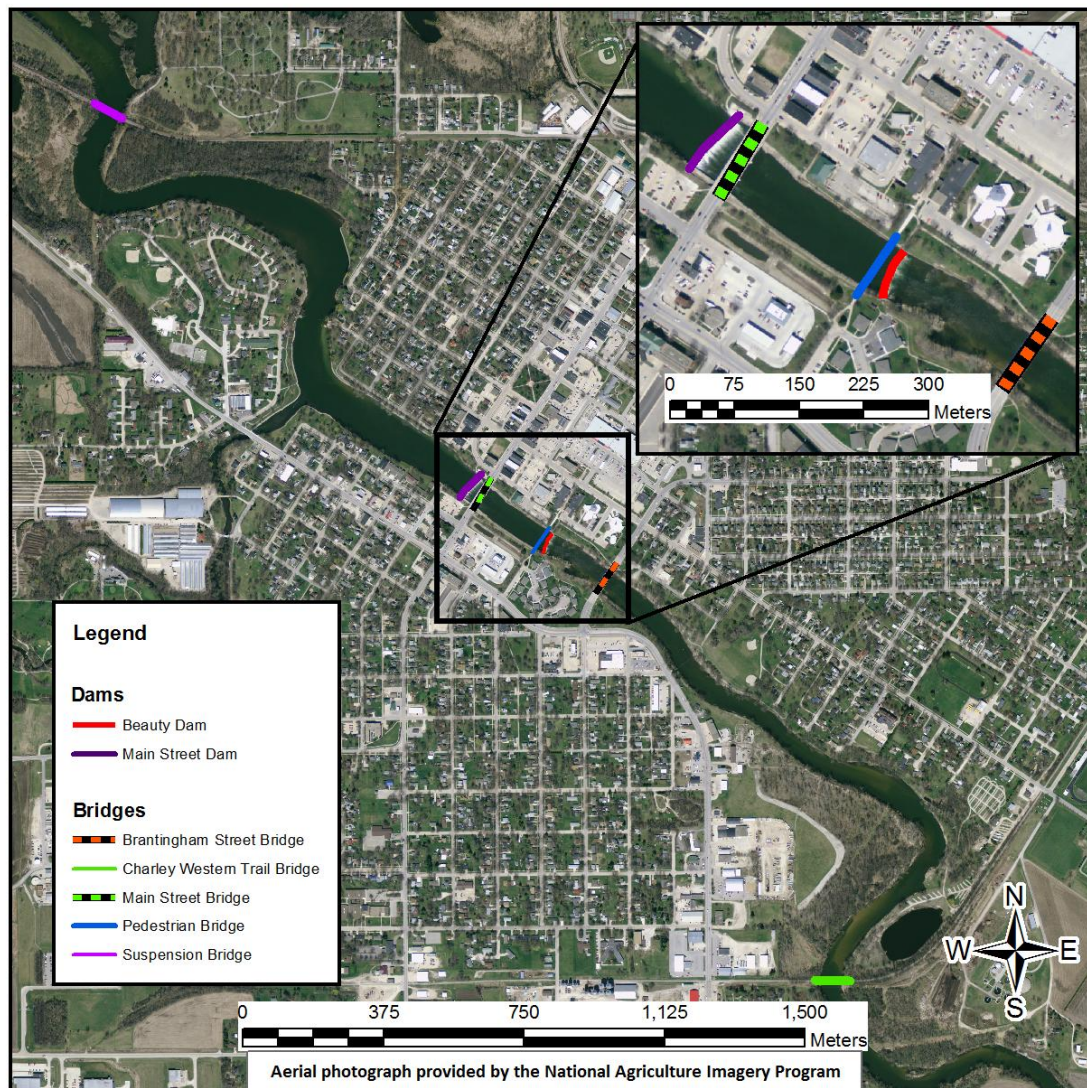


Figure 3.4. Location of structures within the study area.

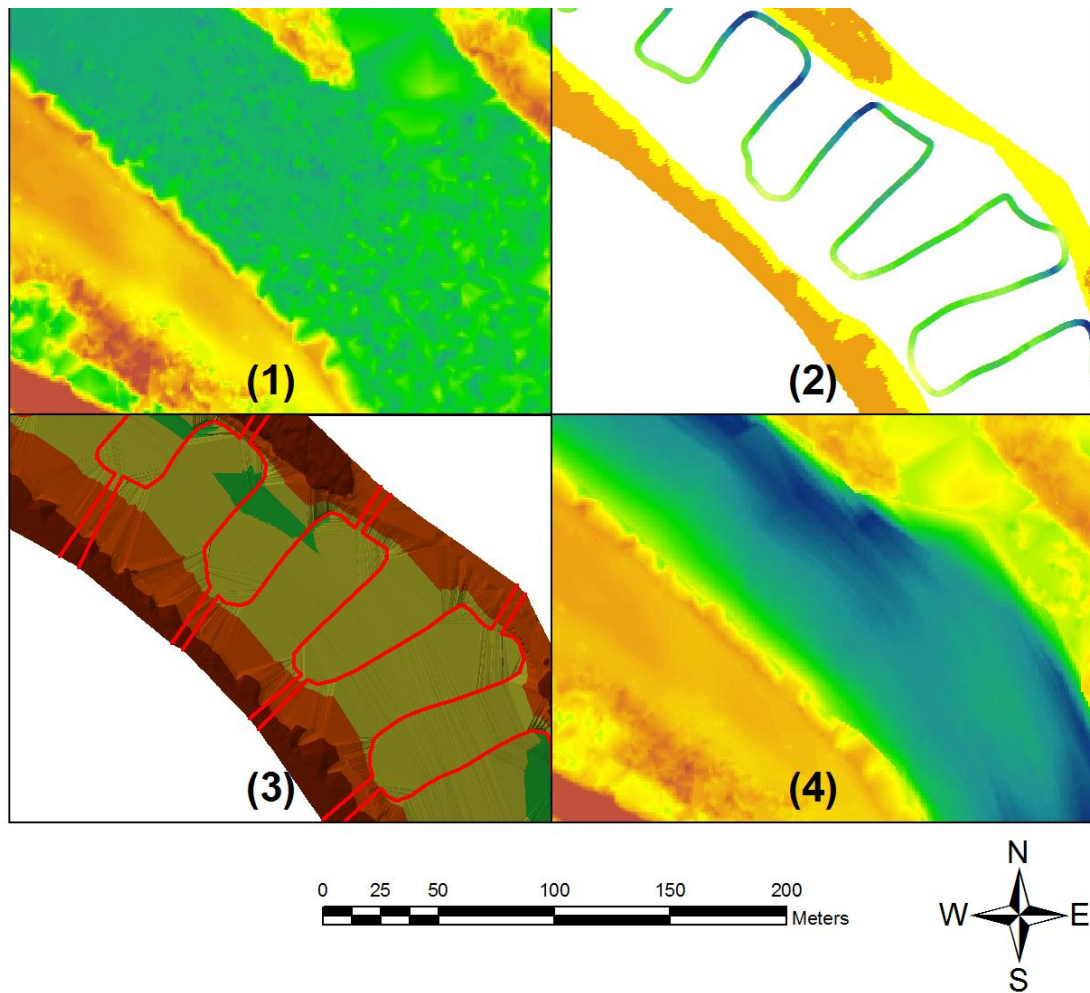


Figure 3.5. The process for merging bathymetry with LiDAR topography. (1) LiDAR topography. (2) The banks are converted to points and merged with channel bathymetry and used to create a TIN. (3) Elevations are extracted to cross-sections using the first TIN. A second TIN is created from extracted cross-section elevations. (4) The second TIN is converted to a raster and merged with the original topography

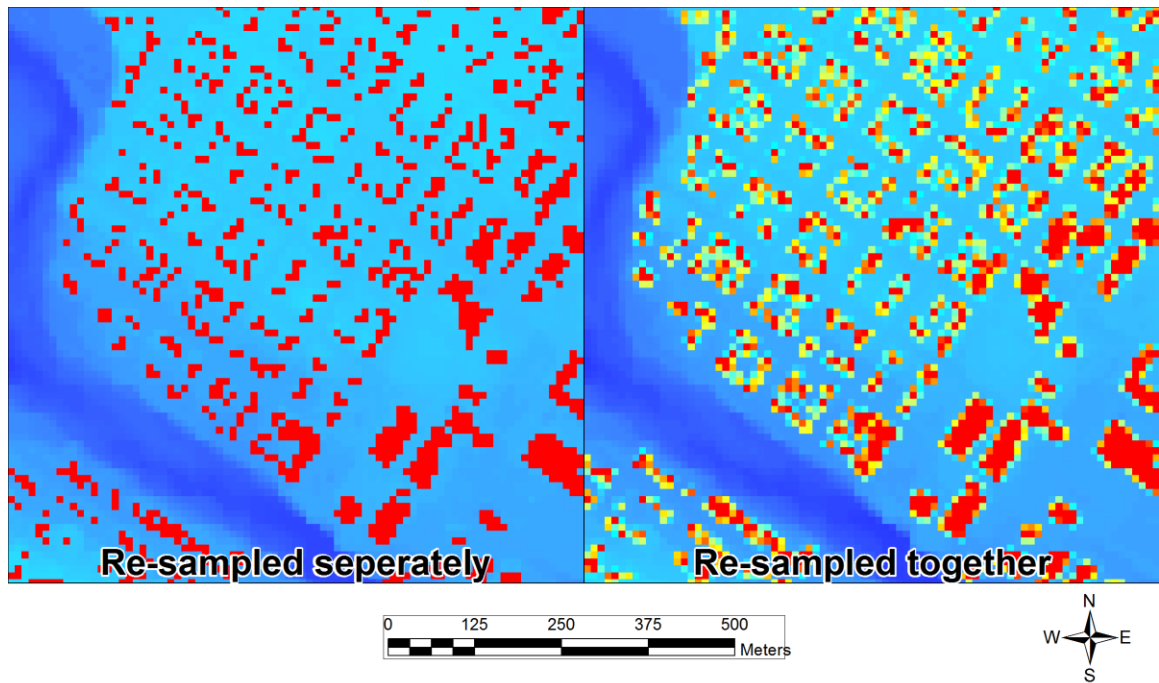


Figure 3.6. Comparison of building footprints. The figure on the left shows building footprints after re-sampling the building raster and DEM to 10 m separately and then merging. The figure on the right shows the building footprints after re-sampling a DEM with buildings already merged to 10 m.

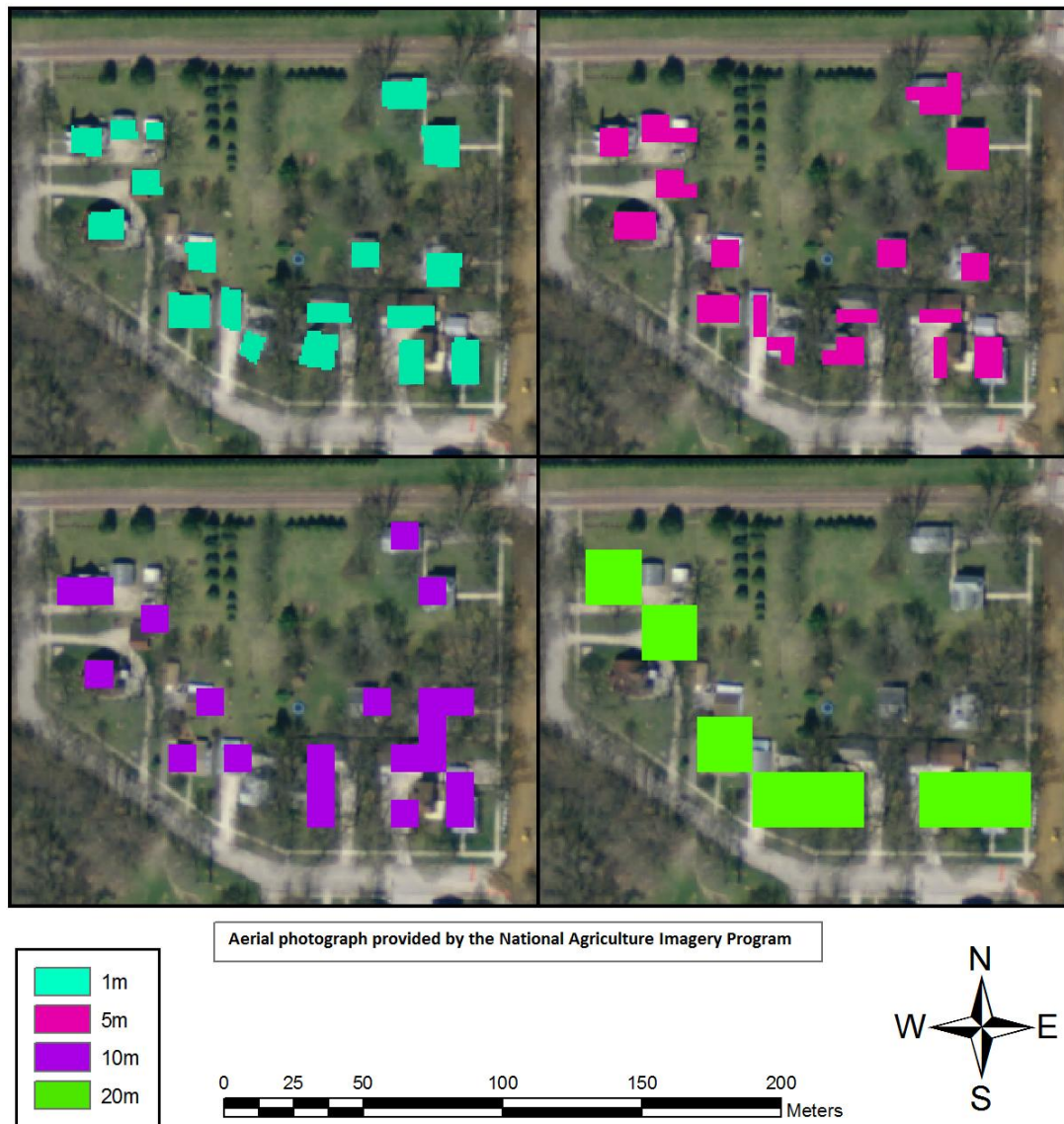


Figure 3.7. Comparison of building footprint distortion with decreasing DEM resolution.

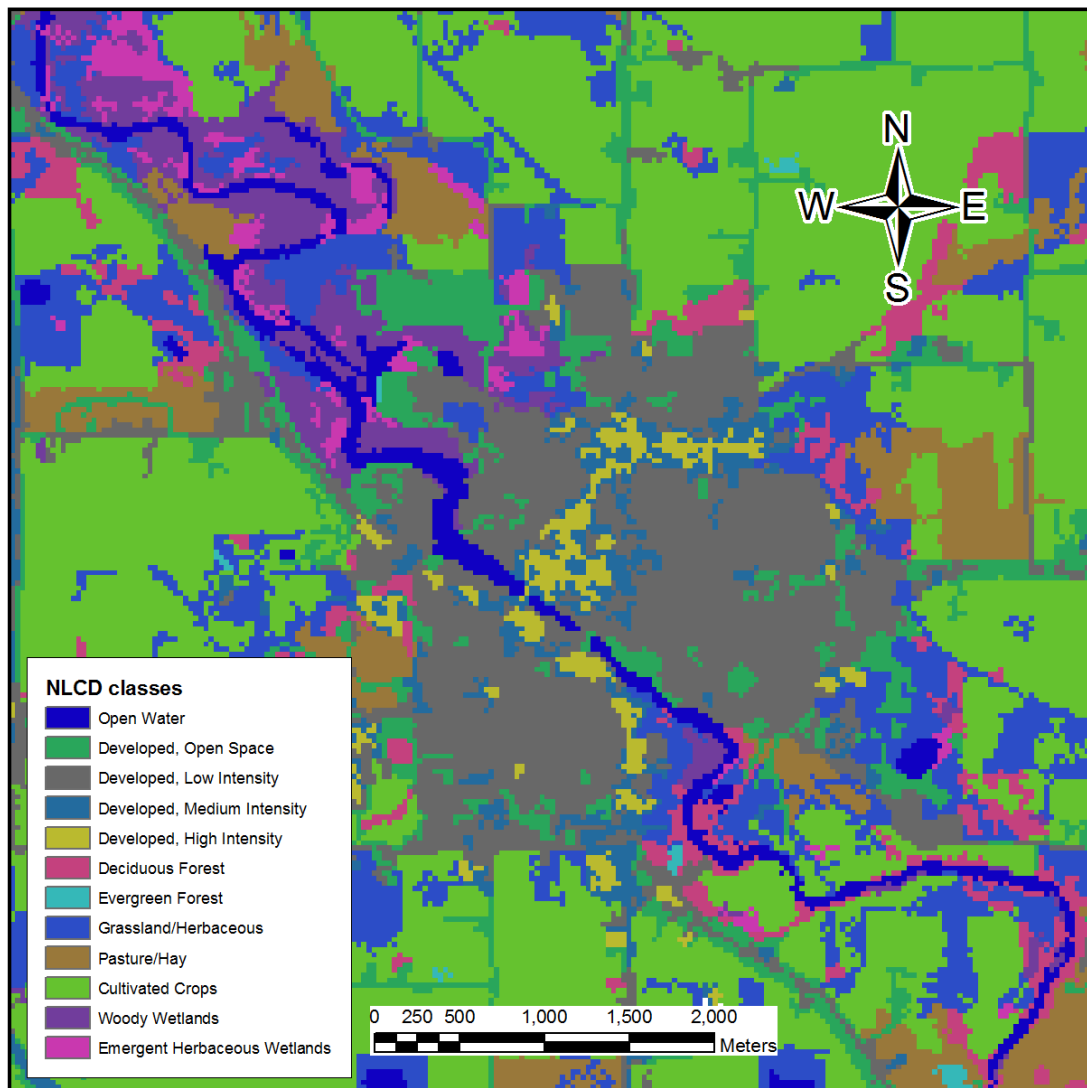


Figure 3.8. Distribution of 2001 National Land Cover Dataset classifications in the study area.

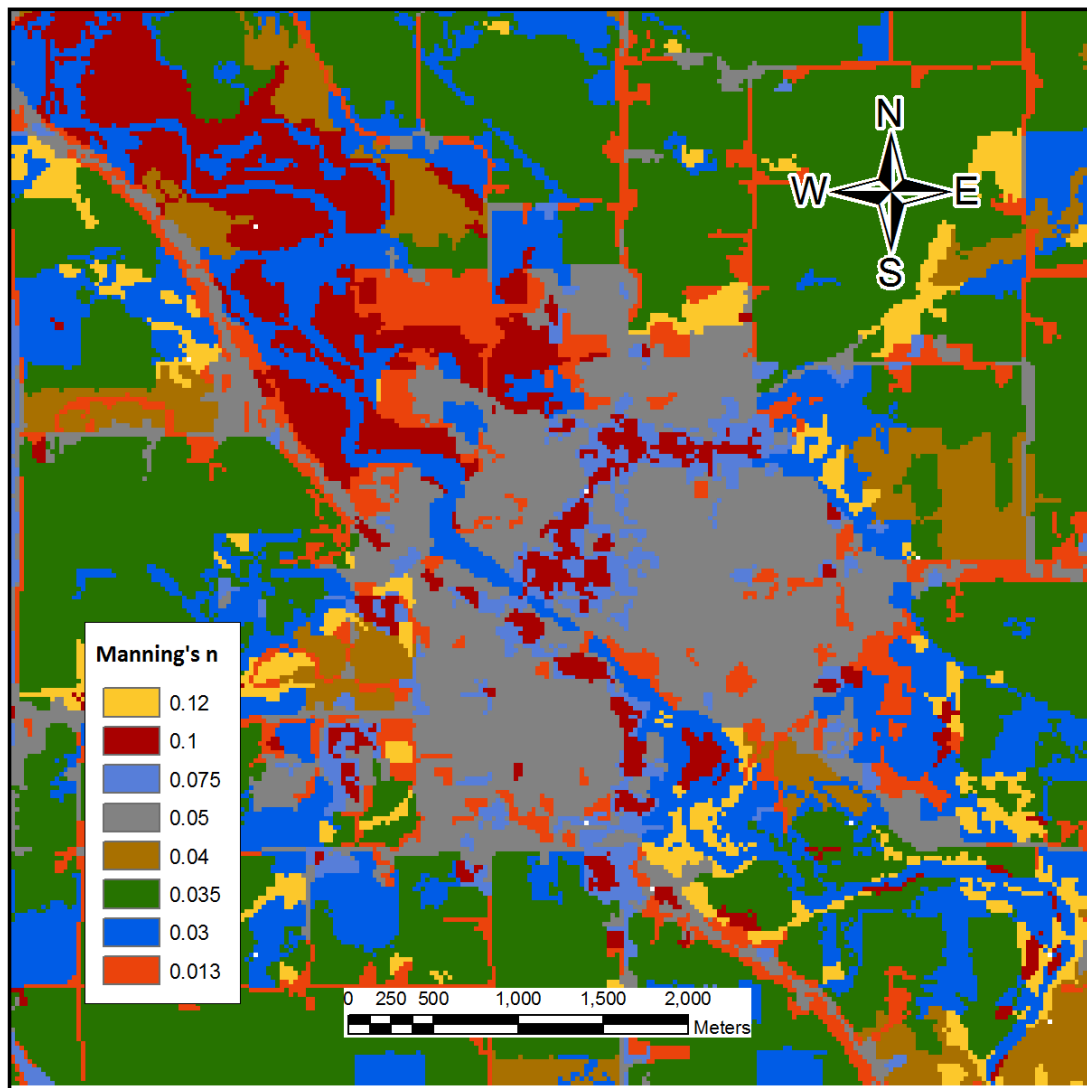


Figure 3.9. Distribution of Manning's "n" roughness parameter based on 2001 NLCD classifications.

Table 3.1. Manning's "n" roughness based on 2001 NLCD classification.

| NLCD Classification | Manning's n | | | Source |
|-----------------------------|-------------|--------|---------|----------------------|
| | Minimum | Normal | Maximum | |
| Open Water | 0.025 | 0.03 | 0.033 | Chow 1959 |
| Developed, Open Space | 0.01 | 0.013 | 0.016 | Calenda, et al. 2005 |
| Developed, Low Intensity | 0.038 | 0.05 | 0.063 | Calenda, et al. 2005 |
| Developed, Medium Intensity | 0.056 | 0.075 | 0.094 | Calenda, et al. 2005 |
| Developed, High Intensity | 0.075 | 0.1 | 0.125 | Calenda, et al. 2005 |
| Barren Land | 0.025 | 0.03 | 0.035 | Chow 1959 |
| Deciduous Forest | 0.1 | 0.12 | 0.16 | Chow 1959 |
| Evergreen Forest | 0.1 | 0.12 | 0.16 | Chow 1959 |
| Mixed Forest | 0.1 | 0.12 | 0.16 | Chow 1959 |
| Scrub/Shrub | 0.035 | 0.05 | 0.07 | Chow 1959 |
| Grassland/Herbaceous | 0.025 | 0.03 | 0.035 | Chow 1959 |
| Pasture/Hay | 0.03 | 0.04 | 0.05 | Chow 1959 |
| Cultivated Crops | 0.025 | 0.035 | 0.045 | Chow 1959 |
| Woody Wetlands | 0.08 | 0.1 | 0.12 | Chow 1959 |
| Emergent Herbaceous Wetland | 0.075 | 0.1 | 0.15 | Chow 1959 |

CHAPTER 4: NUMERICAL SIMULATION

The model DEM was used to extract cross-section geometry for the one-dimensional simulation at 1 m resolution. Bridge and low head dam geometries were then inserted into the 1D model. The 1 m DEM and building rasters were then re-sampled to lower resolution DEMs for the two-dimensional simulation. Water surface elevation data from the bathymetric survey were used to calibrate the 1D model at low flows by adjusting channel roughness. The USGS stream gage rating curve was used to calibrate the model at high flows. A range of surface roughness values from established literature (Table 3.1) were used within the floodplain. Sensitivity analyses were performed to determine the effect of modifying channel roughness, floodplain roughness, eddy viscosity, and mesh density on simulation results. The calibrated model was then used to analyze the effectiveness of re-mapping inundation area using a high-resolution DEM.

4.1 Numerical Methods

Flood conditions were modeled using a coupled 1D/2D numerical simulation. The one-dimensional MIKE11 simulation only included the river channel. Cross-section geometry was extracted from the 1 m resolution model DEM, as shown in Figure 4.1. Cross-sections were placed as near as possible to the original survey transects at a spacing of approximately 30 m. Cross-sections extended from bank to bank, with the exception of the cross-section placed at the outlet. The outlet cross-section covered the floodplain, as no outlets were included in the 2D mesh. This outlet cross section was used to determine a rating curve, which was then used as the downstream boundary condition. Structures were incorporated into the 1D model using as-built plans or survey data.

The 1 m model DEM and distributed roughness raster were re-sampled to 5 m, 10 m, and 20 m resolutions. The building raster was separately re-sampled to the same

resolutions and then merged with the DEM. The coarsened DEMs and roughness raster were then converted to the format used by DHI and imported into MIKE21. An elevation of 350 m was assigned to the buildings as well as a boundary surrounding the 2D model domain. The elevation of 350 m was used as the “land value” within MIKE21. Any cell with an elevation equal to or greater than the land value was removed from the computational domain. The river channel was also removed from the 2D computational domain because the 1D model was used for channel conveyance (Figure 4.2).

The 1D and 2D simulations were coupled using DHI’s MIKE FLOOD software. A number of coupling options were available. The lateral link option was chosen for its simplicity. When using lateral links, structures are modeled entirely within the 1D model and not individually linked to the 2D model. Lateral linkage couples the 1D model to the 2D model by linearly interpolating the endpoints of each cross-section and applying a simple weir equation to model over-topping of the banks. To link the 1D model to the 2D model, the coordinates of the left and right banks of the river network are selected and coupled to the nearest 2D cell. The same node locations were also used to select the cells which are blocked out of the 2D computational mesh. When the two models are coupled, as water elevation increases beyond the extents of each cross-section, the weir equation is applied to model flow exchange between the 1D model and the 2D model.

4.2 Boundary Conditions

In the coupled model, the perimeter of the computational mesh was assigned an elevation of 350 m to close the boundary of the model. It was then only necessary to apply boundary conditions within the 1D model. A downstream rating curve was created assuming normal depth conditions with the distributed roughness and geometry of the outlet cross-section and a slope of 0.0003. The slope was determined by subtracting the bed elevation at the downstream outlet from the bed elevation just downstream of the Charley Western Trail Bridge and dividing by the distance between the two points. The

downstream rating curve was located far downstream of downtown Charles City in an effort to minimize the effect of a normal depth assumption on the simulation results in the area of interest. Bulk flow data from the USGS was used as the inlet boundary condition. Steady discharges corresponding to flow conditions at the time of bathymetric surveys were used for low flow calibration. Steady discharges corresponding to river stages of 12ft, 14 ft, 16 ft, 18 ft, 20 ft, 22 ft, and 24 ft from the USGS rating curve were used for high flow calibration. Selected flow rates begin at the official flood stage of 12 ft as reported by the National Weather Service (NWS) and extend to the peak of the rating curve.

4.3 Structures

The modeled reach contains five bridges and two low head dams. The low head dams were modeled in MIKE11 using the broad crested weir method, as described by Equation 4.3.1.

$$Q_c = \alpha_c 1.705 b H_s^{3/2} \quad (4.3.1)$$

Where Q_c is discharge, α_c is a weir coefficient, b is the width of the weir, and H_s is the depth (DHI, 2009). Two arch bridges, Main Street Bridge and Charley Western Trail Bridge, were within the reach. Initially both arch bridges were modeled using the Hydraulic Research arch bridge method. Initial calibration efforts showed that this method was ineffective for the Charley Western Trail Bridge, the only structure downstream of the USGS stream gage. To correct the inadequate results, the Federal Highway Administration (FHWA) WSPRO method was used for the Charley Western Trail Bridge. The FHWA WSPRO method calculates losses based upon the solution of the energy equation (DHI, 2009). A blockage ratio of 0.1 was used for low flows, and a blockage of 0.6 was used for flows where the water surface elevation was above the level where the arch curvature began, which corresponded to the level at which the inadequate

results occurred. The remaining bridges were modeled using the FHWA WSPRO method.

4.4 Calibration

Very little information was available to calibrate the model. No high water marks were recorded from any of the recent floods in Charles City. Discharge records from the dates of the bathymetric surveys were obtained from the USGS Water Watch website for USGS gage station 05457700 in Charles City. Water surface elevation points were then derived from the locations of bathymetric survey data (Figure 3.3) and used to perform a calibration by modifying channel roughness. The portion of the Cedar River downstream of Beauty Dam was calibrated to the USGS stream gage by adjusting channel roughness. Calibration results are shown in Table 4.1. Sensitivity analyses were conducted to investigate whether other parameters should be adjusted to calibrate the model. It was determined in these sensitivity analyses that the other parameters investigated, eddy viscosity and floodplain roughness, had negligible effect on the results, as discussed in Section 4.5. Distribution of channel roughness is shown in Figure 4.3.

4.5 Sensitivity Analyses

4.5.1 Eddy Viscosity

A sensitivity analysis was conducted using the 10 m mesh to investigate the effect of differing eddy viscosity. DHI recommends calculating eddy viscosity in the 2D simulation by Equation 4.5.1.

$$\varepsilon = \frac{0.02\Delta x \Delta y}{\Delta t} \quad (4.5.1)$$

Where ε is eddy viscosity, Δx and Δy are the mesh resolution in the x and y direction, respectively, and Δt is the time step (DHI 2009). Based on equation 4.5.1, an eddy viscosity of $1.67 \text{ m}^2/\text{s}$ was calculated for the mesh resolution of 10 m and time step of 1.2 seconds. Simulations were run at the initial eddy viscosity of $\varepsilon = 1.67 \text{ m}^2/\text{s}$ as well as $\varepsilon =$

$0.56 \text{ m}^2/\text{s}$ and $\varepsilon = 5 \text{ m}^2/\text{s}$. Results of the sensitivity analysis are shown in Table 4.2. The maximum difference in the water surface profile over the length of the entire reach from $\varepsilon = 1.67 \text{ m}^2/\text{s}$ was only 1.3 cm for $\varepsilon = 0.56 \text{ m}^2/\text{s}$ and 2.9 cm for $\varepsilon = 5 \text{ m}^2/\text{s}$. These values were not considered significant enough to justify varying the eddy viscosity from that recommended by DHI.

4.5.2 Channel Roughness

A sensitivity analysis was conducted to determine the effect of adjusting the channel roughness from the calibrated values by $\pm 15\%$. Results of the simulations are shown in Table 4.3. Reducing and increasing the channel roughness by 15% caused the average water surface elevation to change by almost 40 cm and 30 cm, respectively. This is a considerable difference, and indicates that the results are highly sensitive to the roughness parameter used in the 1D model.

4.5.3 Floodplain Surface Roughness

A sensitivity analysis was conducted using the 10 m mesh to investigate the effect of differing overbank roughness. Chow reports roughness by category as a minimum, normal, and maximum value (Table 3.1). Simulations were performed with all floodplain roughness values set to minimum values, then using normal values and lastly, maximum values. Results of the simulations are shown in Table 4.4. The largest difference from normal roughness in the water surface profile over the length of the entire reach was only 2.5 cm for minimum roughness and 2.4 cm for maximum roughness. These results agree with the findings of Pappenberger et al (2006) that 2D models are relatively insensitive to floodplain roughness. These values were not considered significant enough to justify varying the roughness from the values defined by Chow as “normal”.

4.5.4 Mesh Resolution

Re-sampling the 1 m DEM to coarser resolutions can cause over-simplification of the topography. This is especially apparent when re-sampling the building raster to coarser resolutions as shown in Figure 3.7. Simulations at finer mesh resolutions require significantly more computation time, however. In an effort to strike a balance between a physically consistent topography and computation time, a sensitivity analysis was conducted. Simulations using mesh resolutions of 5 m, 10 m, and 20 m were performed. The simulated flow rates were equivalent to the 10-, 50-, 100-, and 500- year return period flow rates (520 m³/s, 820 m³/s, 920 m³/s, and 1160 m³/s, respectively), as determined using official USGS flow rates using methods described by Eash, 2001. Data from the full period of record through 2010 at USGS stream gage 05457700 were used in the discharge calculations. Simulations at each resolution with buildings removed from the topography were also performed. Eddy viscosity was re-calculated for each simulation using Eq. 4.5.1; all other values were held constant.

To quantify the ability of the model to adequately predict inundation extent at different mesh resolutions, a measure of fit described by Equation 4.5.2 (Bates and De Roo, 2000) was used.

$$Fit = \frac{A_{reference} \cap A_{simulated}}{A_{reference} \cup A_{simulated}} \quad (4.5.2)$$

Where $A_{reference}$ is the inundation extent from the 5 m model with buildings included, and $A_{simulated}$ is the inundation extent of each other model. The 5 m model including buildings was chosen as the reference as it was the most physically consistent of all the simulations. Fit values are presented in Figure 4.4 and Table 4.5. Velocity magnitude in the downtown region of Charles City resulting from each simulation is shown in Figure 4.5. When using the 5 m resolution mesh for baseline comparison, the most significant differences in inundation extent occur in the downtown area at high flow rates, as shown in Figure 4.6. Inundation area for all flows decreased as mesh resolution

decreased, especially at higher flow rates. Differences in inundation area for each model are shown in Figure 4.7. The effect of removing buildings from each model is shown in Figure 4.8. Removing buildings had a considerable effect on the inundation extent for high flows, as inundation area was considerably larger with buildings incorporated into the model. The difference in inundation area is less apparent at a resolution of 20 m when buildings were removed from the model.

A re-sampling tool was later used on the results from these simulations to determine whether it would be feasible to reliably improve coarse mesh simulation results to within an acceptable degree of accuracy as compared to results using a finer mesh as discussed in Chapter 5.

4.6 Summary

A coupled 1D/2D numerical hydraulic model of Charles City was developed to simulate flood events. The 1D MIKE11 model was coupled to the 2D MIKE21 model using lateral links, which approximate exchange of water between the river channel and the floodplain using a simplified weir equation. All of the structures within the reach, five bridges and two low-head dams, were included in the 1D model. The model was calibrated using a rating curve from the USGS stream gage and measured water surface elevations from bathymetric surveys. Sensitivity analyses were performed to investigate the effect of modifying eddy viscosity, floodplain roughness, and mesh resolution.

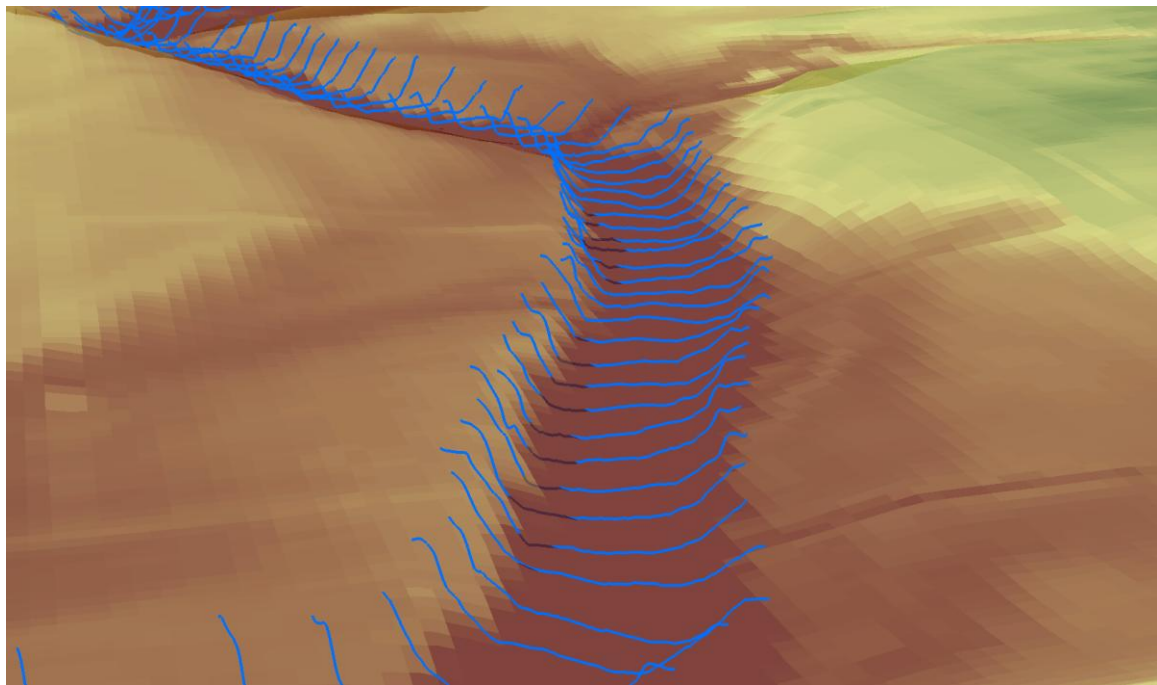


Figure 4.1. 3D representation of cross-section extraction from DEM.

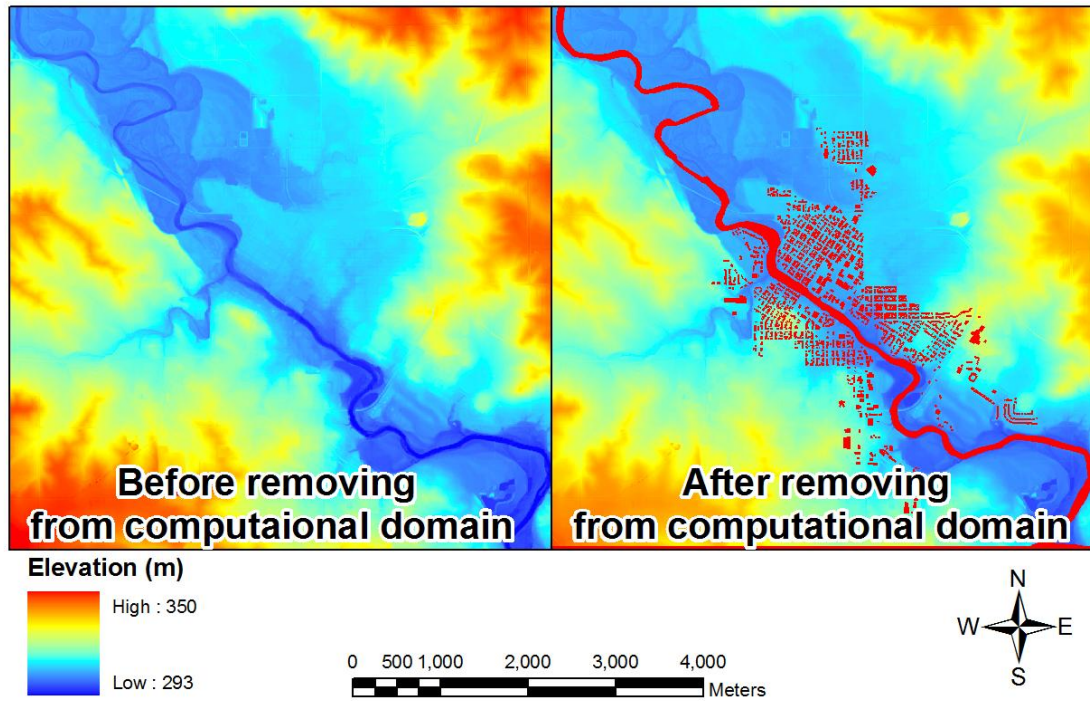


Figure 4.2. Removal of buildings and river channel form computational mesh.

Table 4.1. Difference in water surface elevation at USGS stream gage 05457700 after model calibration.

| Q (m^3/s) | WSE, simulated (m) | WSE, rating curve (m) | Difference (m) |
|-------------------------------|--------------------|-----------------------|----------------|
| 280 | 300.498 | 300.247 | 0.251 |
| 350 | 301.027 | 300.857 | 0.17 |
| 430 | 301.549 | 301.466 | 0.083 |
| 510 | 302.214 | 302.076 | 0.138 |
| 610 | 302.72 | 302.685 | 0.035 |
| 720 | 303.212 | 303.295 | 0.083 |
| 860 | 303.793 | 303.905 | 0.112 |
| Standard Deviation, m | | | 0.071 |

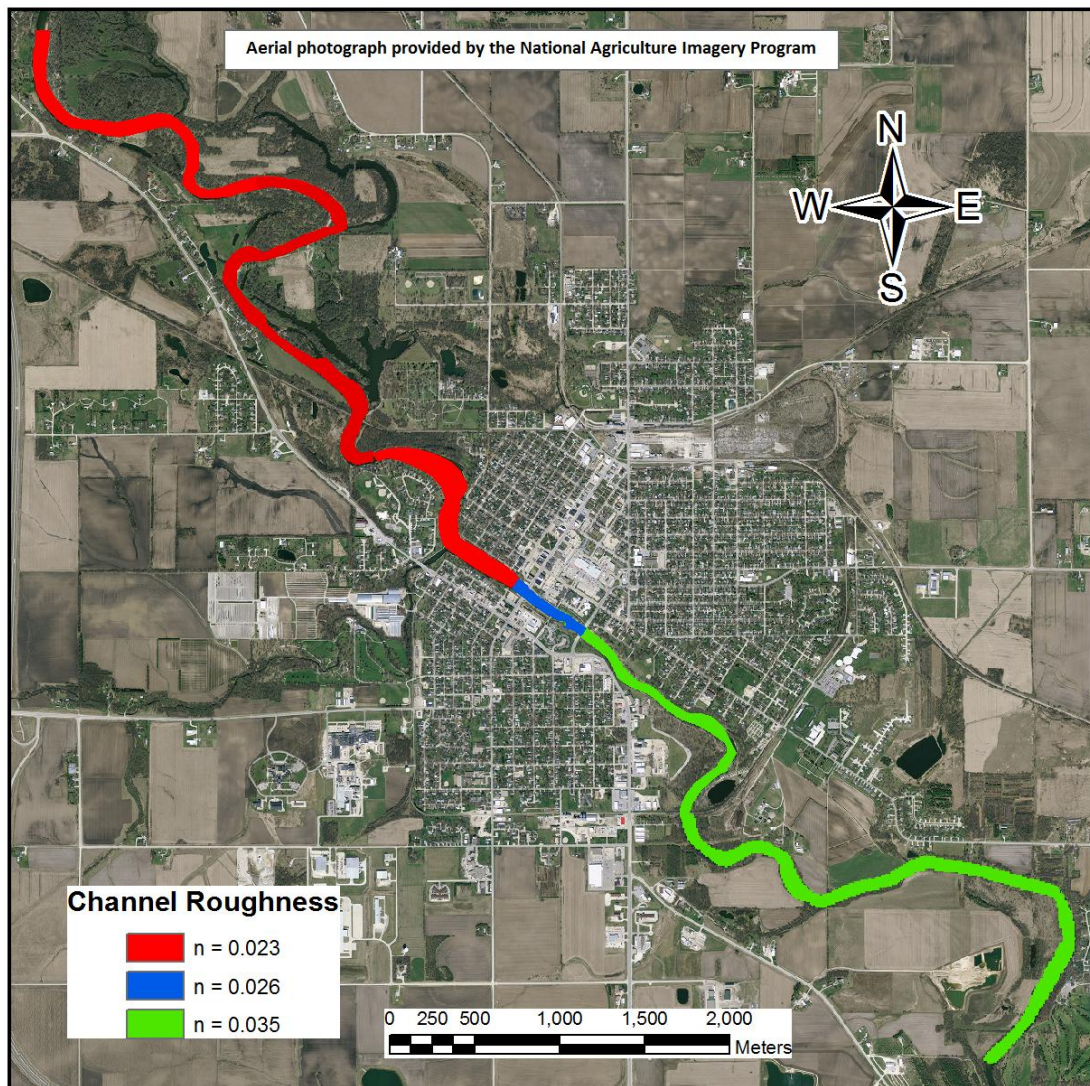


Figure 4.3. Distribution of calibrated channel roughness within the study area.

Table 4.2. Eddy viscosity sensitivity analysis results. The difference in overall water surface elevation from the results using $\varepsilon = 1.67 \text{ m}^2/\text{s}$ are shown.

| Discharge (m^3/s) | $\varepsilon = 0.5 \text{ m}^2/\text{s}$ | | $\varepsilon = 5 \text{ m}^2/\text{s}$ | |
|--|--|--------------------|--|--------------------|
| | Avg. Difference (m) | Std. Deviation (m) | Avg. Difference (m) | Std. Deviation (m) |
| 280 | 0.009 | 0.059 | 0.006 | 0.071 |
| 350 | 0.012 | 0.016 | 0.012 | 0.064 |
| 430 | 0.011 | 0.018 | 0.015 | 0.017 |
| 510 | 0.015 | 0.018 | 0.016 | 0.029 |
| 610 | 0.022 | 0.024 | 0.019 | 0.024 |
| 720 | 0.025 | 0.021 | 0.024 | 0.026 |

Table 4.3. Channel roughness sensitivity analysis results. The difference in overall water surface elevation from the results using the calibrated channel roughness values are shown.

| Discharge (m^3/s) | Channel roughness decreased by 15% | | Channel roughness increased by 15% | |
|-------------------------------------|------------------------------------|--------------------|------------------------------------|--------------------|
| | Avg. Difference (m) | Std. Deviation (m) | Avg. Difference (m) | Std. Deviation (m) |
| 280 | 0.214 | 0.138 | 0.144 | 0.091 |
| 350 | 0.244 | 0.166 | 0.161 | 0.076 |
| 430 | 0.193 | 0.097 | 0.142 | 0.104 |
| 510 | 0.361 | 0.147 | 0.209 | 0.055 |
| 610 | 0.387 | 0.138 | 0.268 | 0.091 |
| 720 | 0.249 | 0.087 | 0.152 | 0.110 |

Table 4.4. Floodplain roughness sensitivity analysis results. The difference in overall water surface elevation from the results using the normal floodplain roughness values are shown.

| Discharge (m ³ /s) | Minimum Roughness | | Maximum Roughness | |
|-------------------------------|---------------------|--------------------|---------------------|--------------------|
| | Avg. Difference (m) | Std. Deviation (m) | Avg. Difference (m) | Std. Deviation (m) |
| 280 | 0.009 | 0.059 | 0.006 | 0.071 |
| 350 | 0.012 | 0.016 | 0.012 | 0.064 |
| 430 | 0.011 | 0.018 | 0.015 | 0.017 |
| 510 | 0.015 | 0.018 | 0.016 | 0.029 |
| 610 | 0.022 | 0.024 | 0.019 | 0.024 |
| 720 | 0.025 | 0.021 | 0.024 | 0.026 |

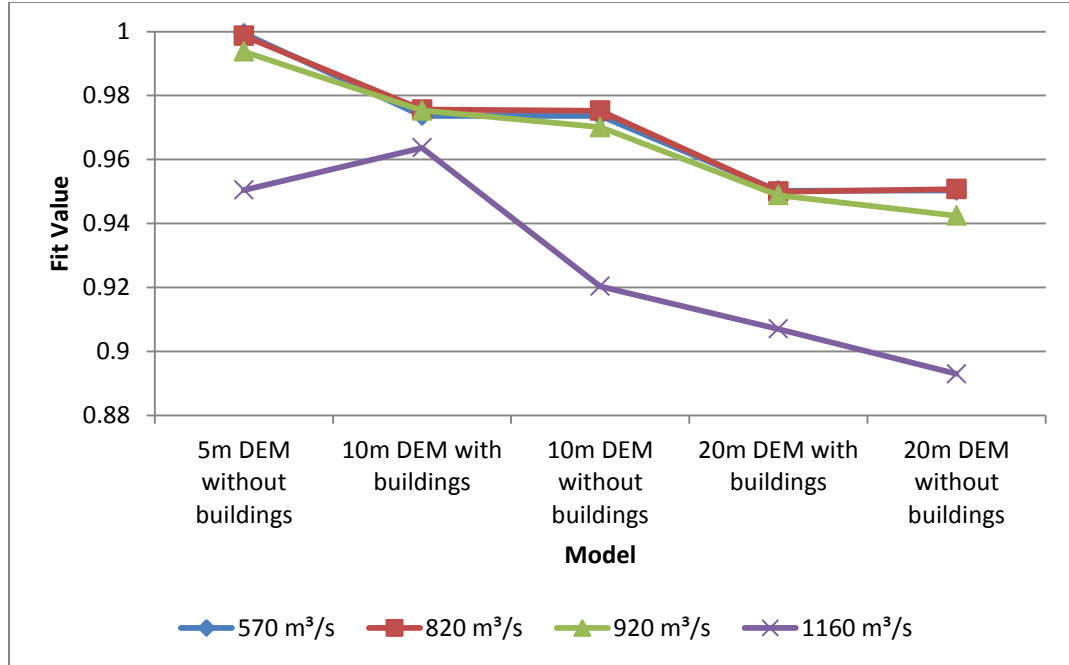


Figure 4.4. Fit values as compared to simulation results from the 5 m model including buildings before re-sampling.

Table 4.5. Fit value as compared to simulation results from the 5 m model including buildings before re-sampling.

| Discharge | 570 m³/s | 820 m³/s | 920 m³/s | 1160 m³/s |
|-----------------------|----------|----------|----------|-----------|
| 5m without buildings | 0.999 | 0.999 | 0.994 | 0.950 |
| 10m without buildings | 0.974 | 0.975 | 0.970 | 0.920 |
| 10m with buildings | 0.974 | 0.976 | 0.975 | 0.964 |
| 20m without buildings | 0.950 | 0.951 | 0.942 | 0.893 |
| 20m with buildings | 0.950 | 0.950 | 0.949 | 0.907 |

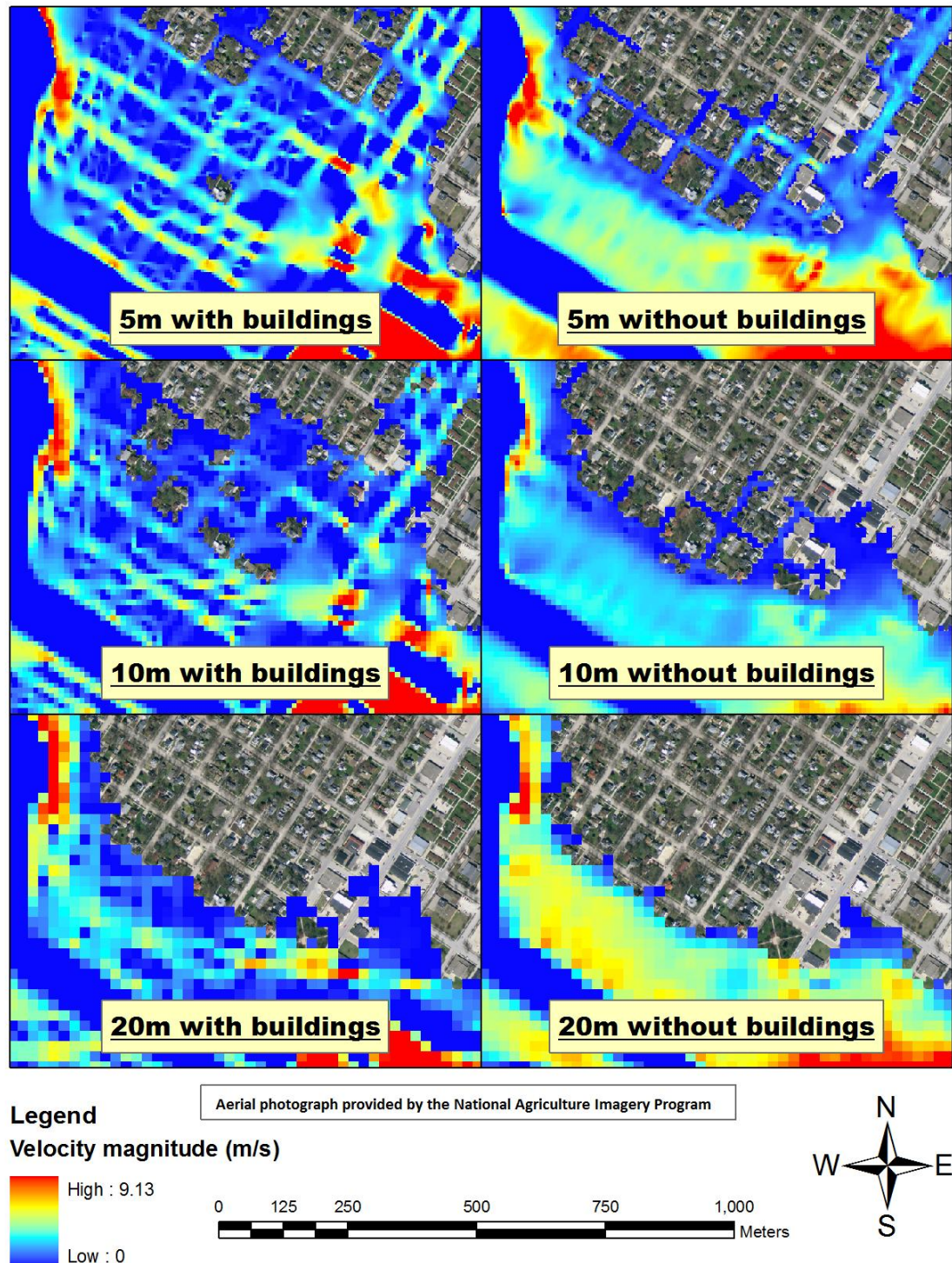


Figure 4.5. Distribution of velocity magnitude at $Q = 1160 \text{ m}^3/\text{s}$ in downtown Charles City.

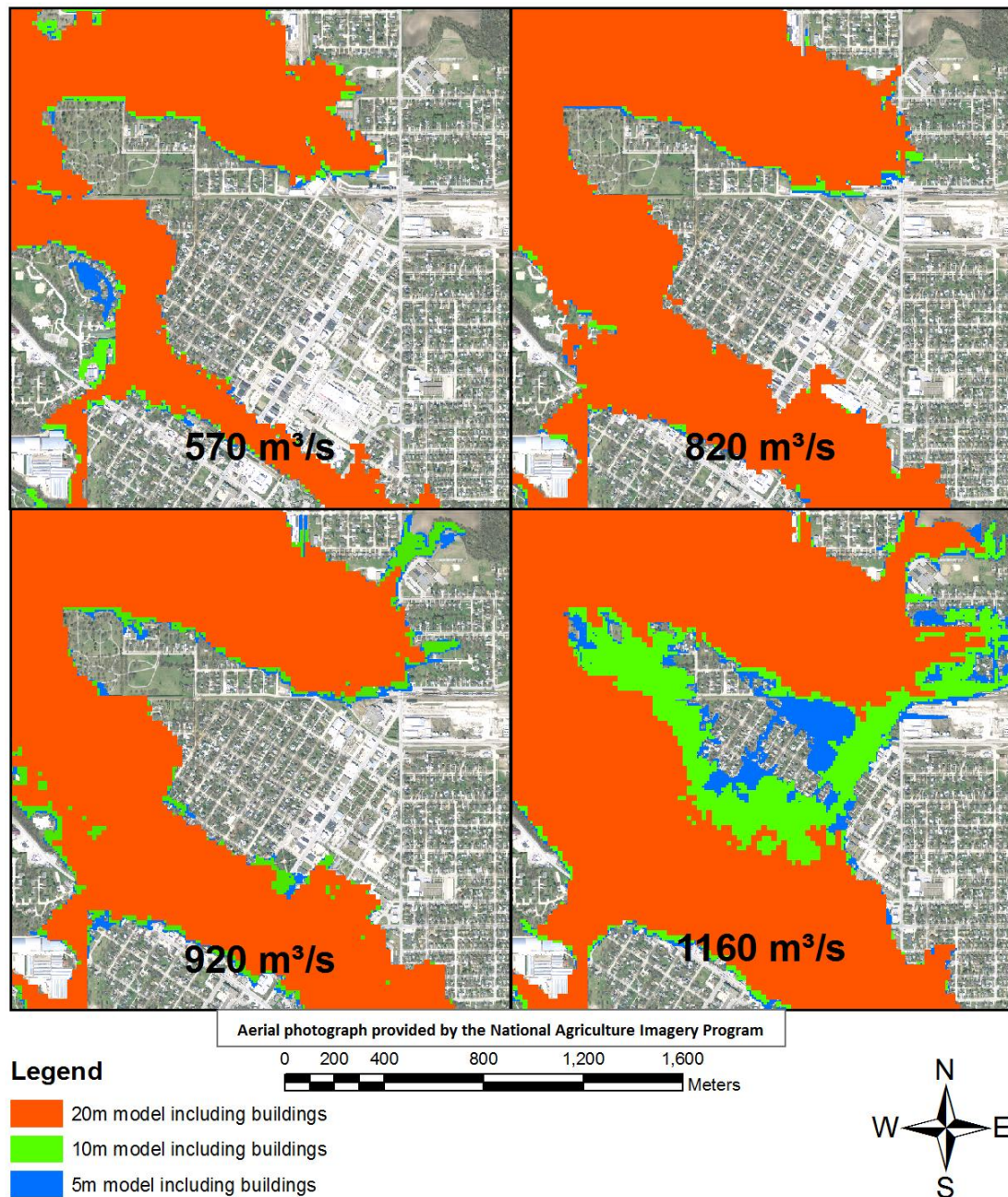


Figure 4.6. Inundation differences from models including buildings in the downtown region of Charles City.

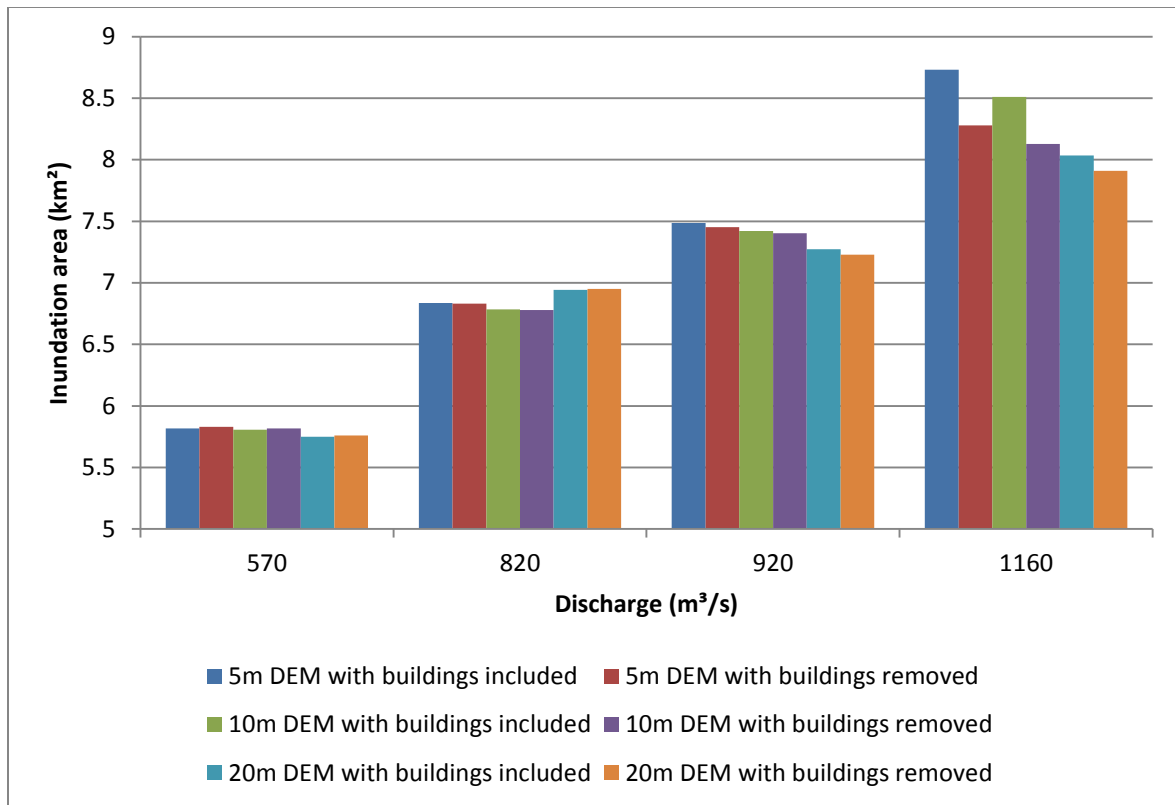


Figure 4.7. Difference in inundation area for each model.

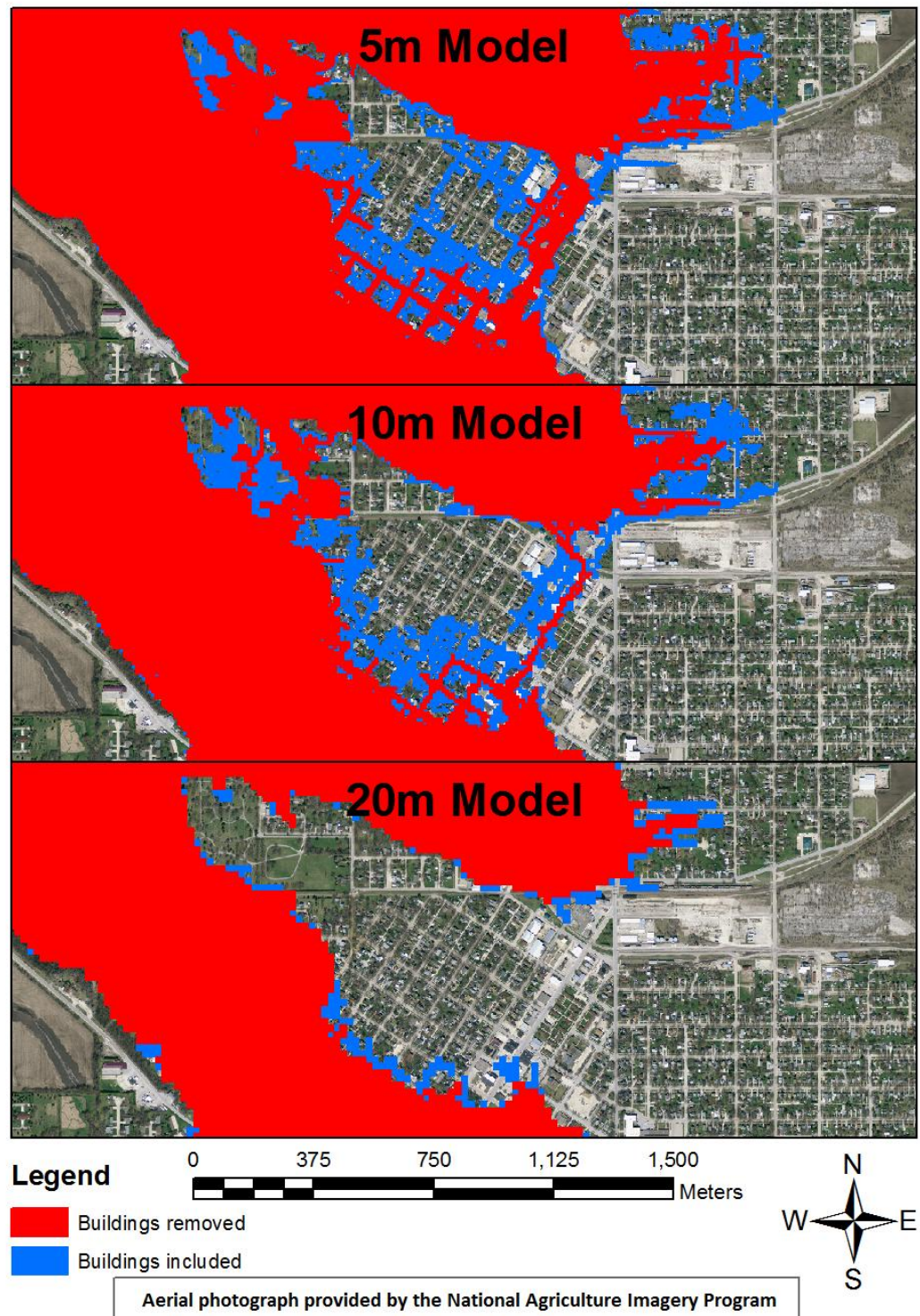


Figure 4.8. Simulation results at a discharge of $1160 \text{ m}^3/\text{s}$ from models at 5m, 10 m, and 20 m resolutions with buildings included and removed.

CHAPTER 5: HIGH-RESOLUTION RE-SAMPLING RESULTS

Simulation results were re-sampled to improve inundation resolution, as shown in Figure 5.1. A buffer distance of 15 m was used to isolate the cells on the perimeter of the inundation extent. The raster cells on the perimeter were then converted to water surface elevation points. An inverse distance weighted spatial algorithm was used to extrapolate water surface elevation from the perimeter water surface elevation points to adjacent dry cells. This ensured that the inundation extent was not under-predicted when the DEM was subtracted from the water surface. The extrapolated water surface elevation data was then combined with the original water surface elevation raster. The high-resolution (1m) DEM was then subtracted from the combined water surface elevation to create a new, high-resolution depth raster. Disconnected pools, artificially created by the IDW algorithm, were removed from the depth raster.

5.1 Effect of the re-sampling tool

Simulations were performed at $570 \text{ m}^3/\text{s}$, $820 \text{ m}^3/\text{s}$, $920 \text{ m}^3/\text{s}$, and $1160 \text{ m}^3/\text{s}$ for each mesh resolution of 5 m, 10 m, and 20 m. Simulations at the same discharges were also run with buildings removed from each model. Changes in inundation extent are most apparent in the downtown region of Charles City as shown in Figure 5.2. Differences in inundation area for each model are shown in Figure 5.3. Total inundation area increased for all results after using the re-sampling tool; however, inundation area was consistently larger when using a higher-resolution model. The consistent increase in inundation area may be specific to this study area. Inundation areas for each simulation before and after using the re-sampling tool are shown in Figure 5.4-5.7. Inundation area increased for all simulation results after re-sampling. The overall trends of the simulation results were unchanged by re-sampling. The difference in inundation extent due to re-sampling at an increased resolution can be explained by the example cross-section shown in Figure 5.8. The water surface meets the simplified topography of the coarse resolution

mesh sooner than it would have using the finer mesh, reducing the inundation extent. The consistent increase in inundation area may be due to the complex topography found in urban settings. Figure 5.9 and 5.10 compare topography by comparing cross-sectional elevations extracted from both fine- and coarse-resolution DEMs. The cross-section extracted from a fine resolution DEM has a large area for conveyance in the street. This area is significantly reduced when extracting from a coarse-resolution DEM.

Equation 4.5.2 was used to determine the quality of “fit” for each simulation. The results from the 5 m model with buildings included were used for reference. Fit values for all simulations improved after using the re-sampling tool. Fit values are shown in Figure 5.11-5.12, and Table 5.1. In all cases, the fit value increased from the initial pre-processed values. Fit value decreased with increasing discharge. This is likely due to the resolution of each model being unable to accurately capture the complex urban terrain. Differences in depth are more apparent, as the re-sampling tool makes no adjustment to the overall water surface elevation. Differences in depth are shown in Figure 5.13-5.18. The 5m model with buildings removed typically has the highest correlation with the 5 m model with buildings included. Depths at the extreme limits of the dataset show a nearly 1:1 relationship. The deepest depths occur in the stream channel; most of the shallowest depths should occur at the boundary of the inundation. A larger spread in values occurred near the midpoint of the dataset. The other models also had a high correlation of depths in the stream channel, but a larger spread in values at low depths. This is likely due to the different inundation extents resulting from each model. The most consistent overall depth results compared to the results from the 5 m model with buildings included came from the 10 m model with buildings included, with an average difference in depth of less than 0.1 m for all simulated flow rates.

The primary advantage of the re-sampling tool is the ability to use a lower resolution mesh to achieve results that are comparable to using a higher resolution mesh. The potential time savings of decreasing resolution are substantial. Run times for the

simulations investigated in this paper are shown in Table 5.3. A three day steady hydrograph was used for all flows. While the 5 m simulations required several days to run, the 10 m simulations were completed in a few hours, and the 20 m simulations were completed in an hour or less. The fit value may be used as a criterion for selecting minimum acceptable mesh resolution. Depending upon the threshold of fit determined to be acceptable, a model providing the best balance between accuracy of results and simulation time may be selected. In the case of the Charles City models, with a fit value threshold of 0.975, the 10 m model with buildings included can provide results which are comparable to a 5 m resolution model while reducing computation time by approximately a factor of ten. With a fit value threshold of 0.925, the 20 m model with buildings included can provide results which are comparable to a 5 m resolution model while reducing computation time by approximately a factor of 80.

5.2 Model Application

Development of this 1D/2D coupled numerical model was inspired by the damage caused during the 2008 floods. Alterations were made to the model developed for this paper to incorporate changes to the stream channel which are planned in downtown Charles City. The resulting model was used to create a library of inundation maps using steady flow conditions. These maps are available to the public on the Iowa Flood Center website (Figure 5.19). The maps were made to correspond with stage increments on the USGS gage to give the user an idea of how a forecasted stage may affect them. It is hoped that these maps will help residents of Charles City, as well as the city planners, to evaluate risk associated with floods.

5.3 Summary

A re-sampling tool was applied to the simulation results to improve accuracy. The re-sampling tool uses inverse distance weighting to interpolate inundation from a 1 m DEM of the study area. The tool also fills gaps in the inundation area and removes

disconnected areas. When applied to the simulation results from the Charles City models, fit values and inundation area for all simulations increased. The tool may be used to determine a resolution that will provide accurate results without the expense of a significantly large simulation time.

After modifying the model developed for this paper to account for stream channel changes in downtown Charles City, steady flow simulations were run to create a library of inundation maps. These inundation maps are available to the public on the Iowa Flood Center website. It is hoped the maps will help residents and planners in Charles City make informed decisions about potential flood risk.

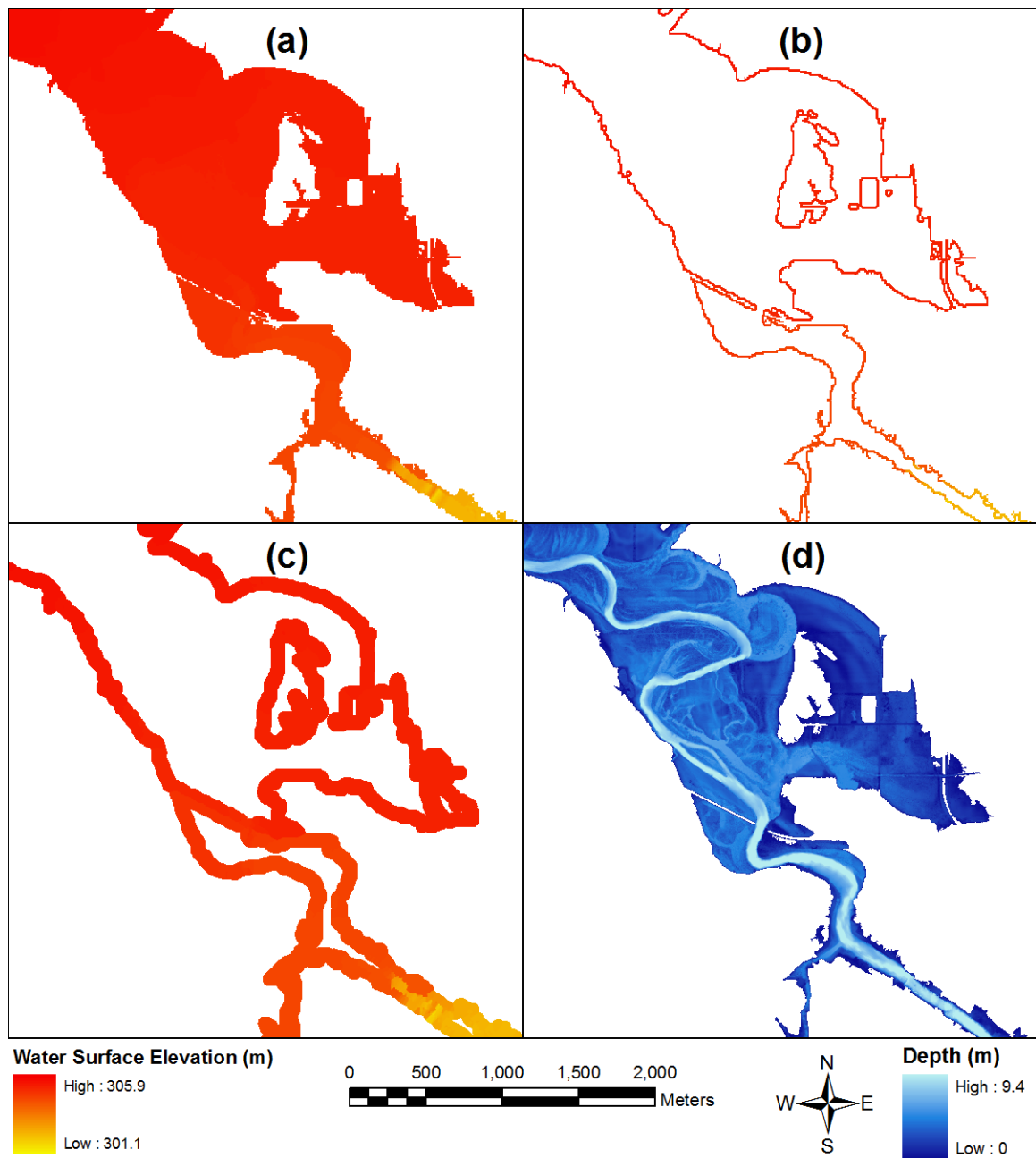


Figure 5.1. The re-sampling process is shown. (a) Water surface elevation (WSE) result files at the original resolution. (b) The boundary of the WSE are selected and converted to points. (c) WSE is extrapolated from the boundary points using an IDW algorithm. (d) The extrapolated points are combined with the original WSE raster. DEM elevations are subtracted from the combined WSE raster. Negative depth values and disconnected areas are removed.

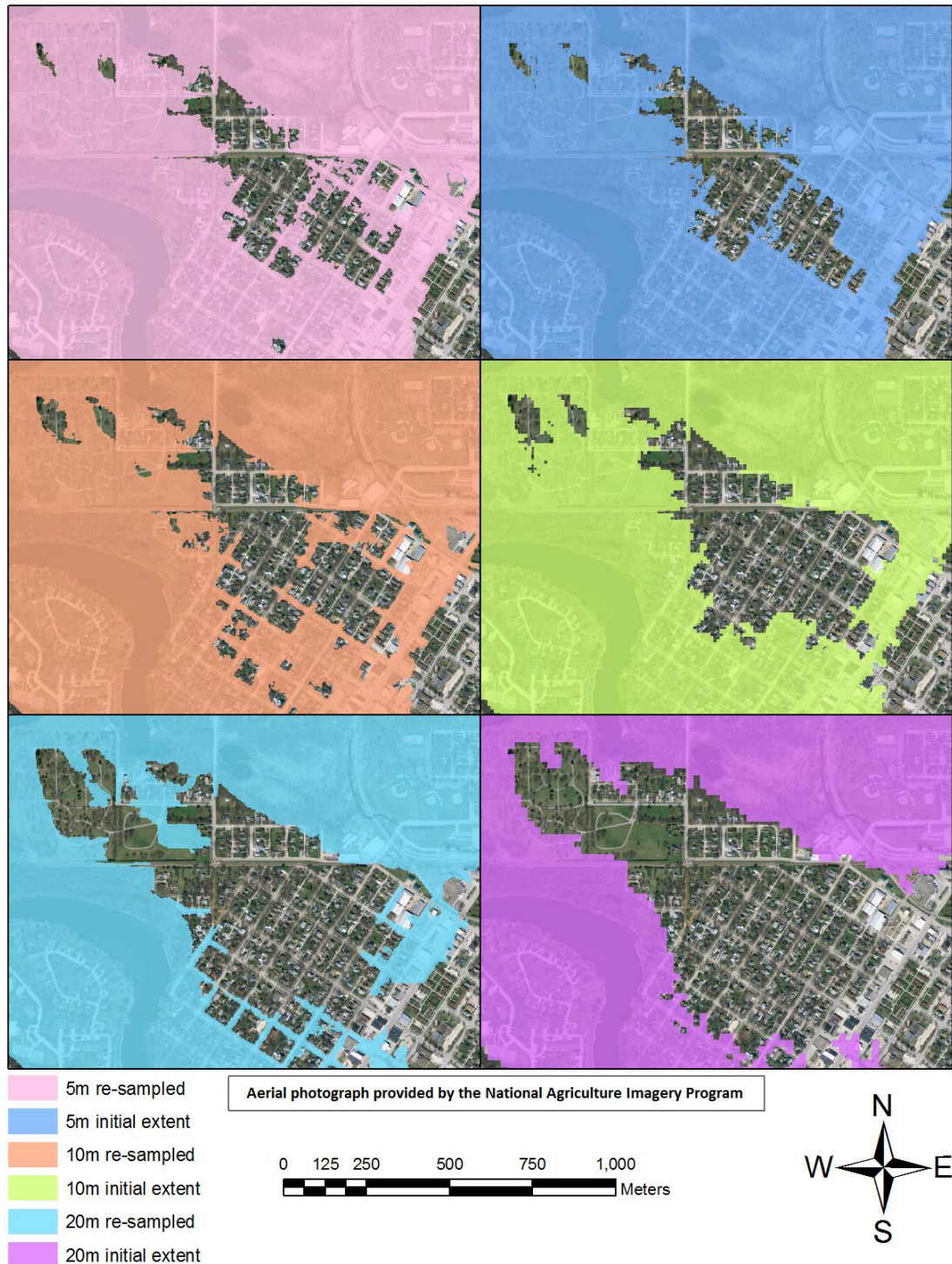


Figure 5.2. Inundation areas after and before re-sampling at a discharge of $1160 \text{ m}^3/\text{s}$. Significant increases in inundation occur after re-sampling the simulation results

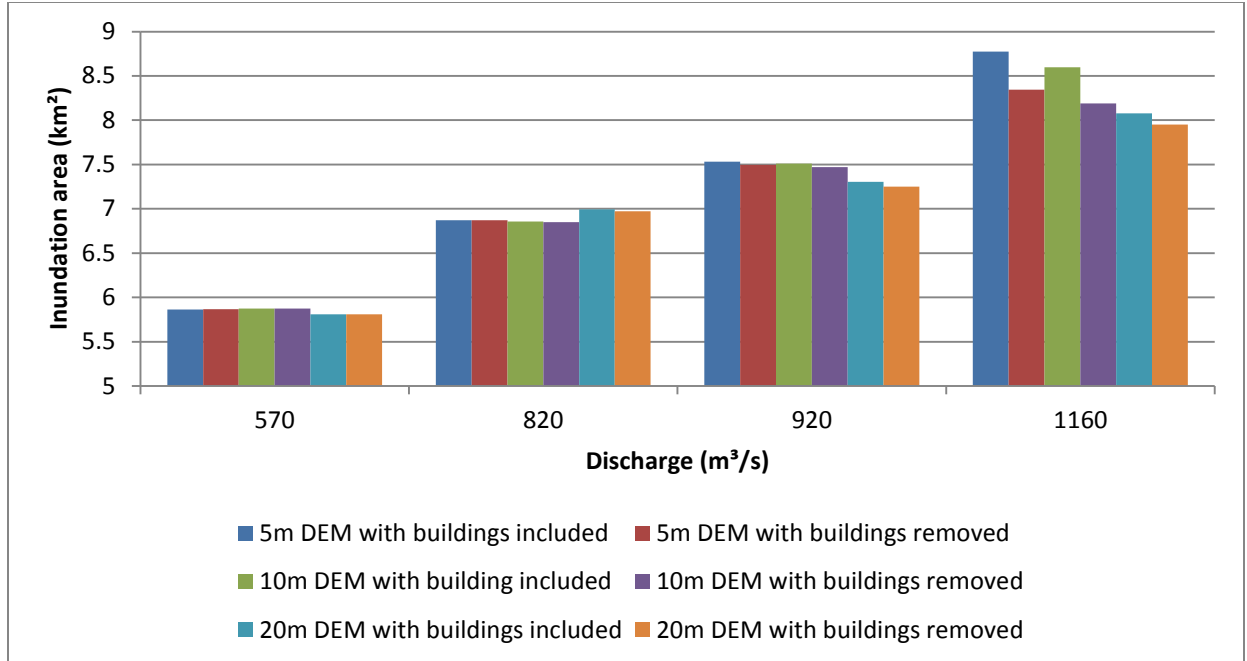


Figure 5.3. Difference in inundation area for each simulation after re-sampling.

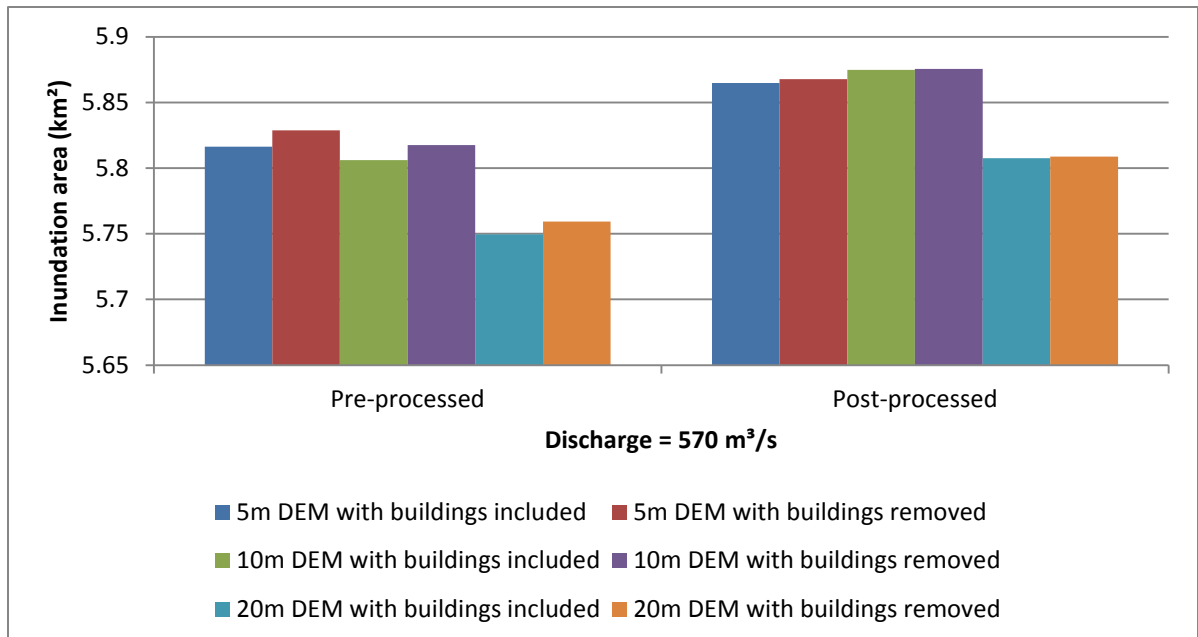


Figure 5.4. Difference in inundation area before and after using the re-sampling tool at a discharge of 570 m³/s.

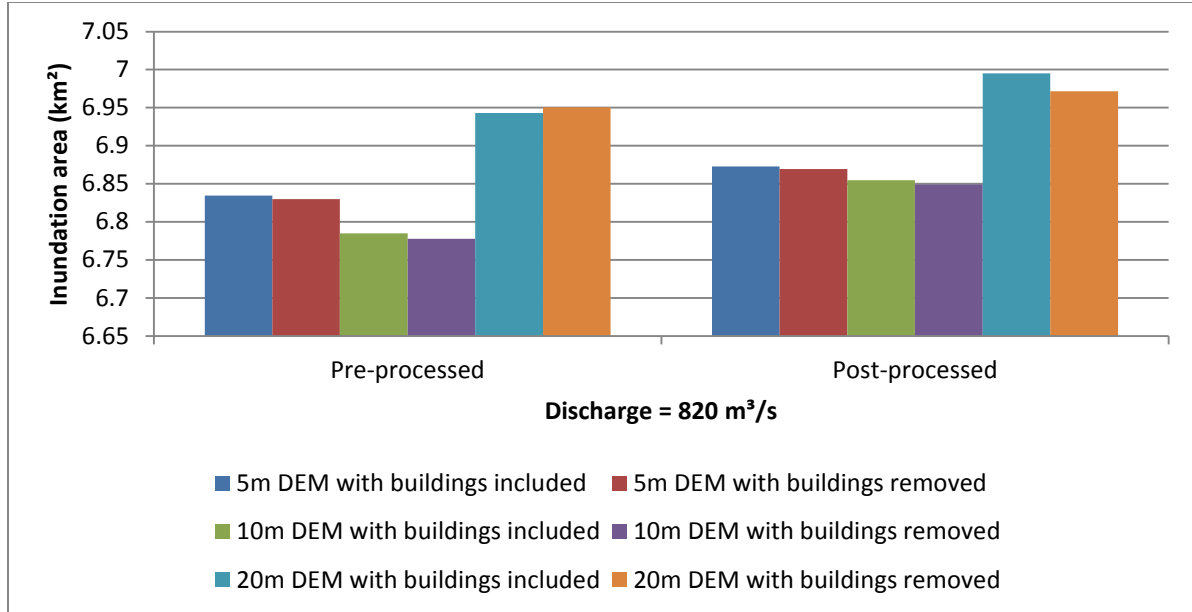


Figure 5.5. Difference in inundation area before and after using the re-sampling tool at a discharge of $820 \text{ m}^3/\text{s}$.

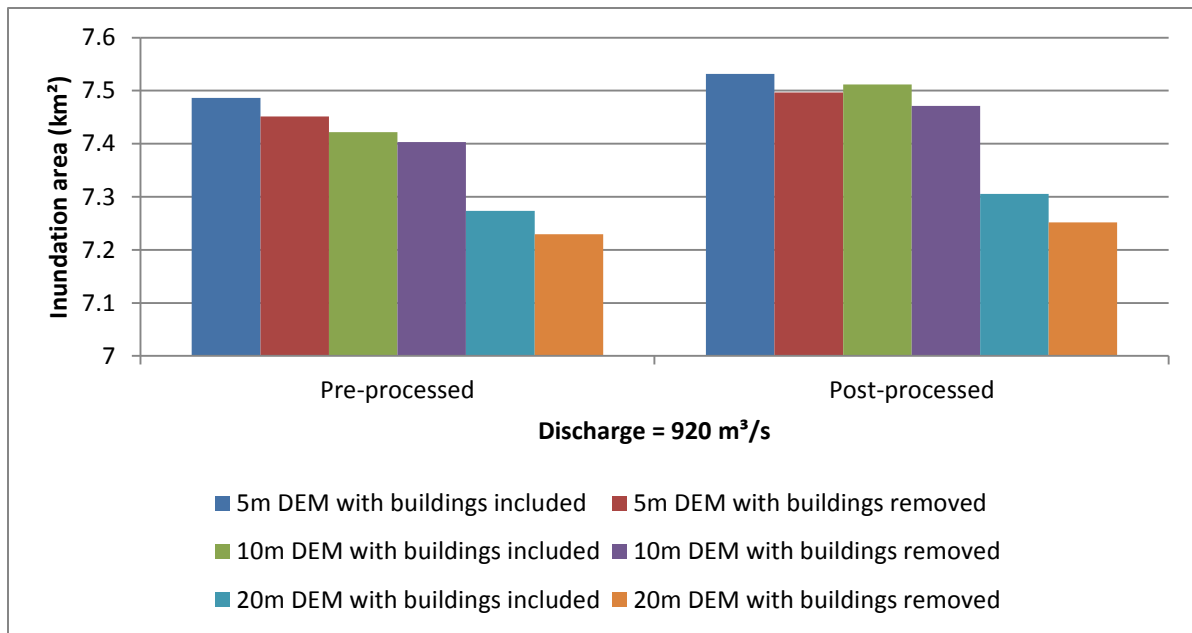


Figure 5.6. Difference in inundation area before and after using the re-sampling tool at a discharge of $920 \text{ m}^3/\text{s}$.

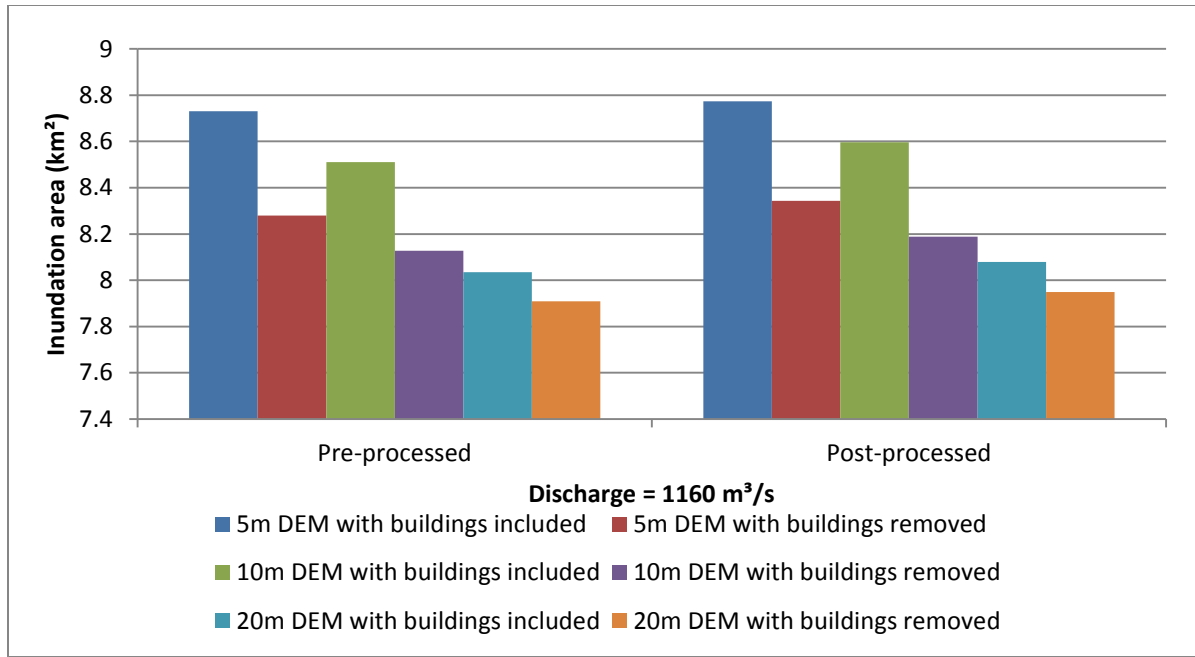


Figure 5.7. Difference in inundation area before and after using the re-sampling tool at a discharge of $1160 \text{ m}^3/\text{s}$.

Table 5.1. Fit value as compared to simulation results from the 5 m model including buildings after re-sampling.

| Discharge | 570 m^3/s | 820 m^3/s | 920 m^3/s | 1160 m^3/s |
|-----------------------|---------------------------|---------------------------|---------------------------|----------------------------|
| 5m without buildings | 1.000 | 0.994 | 0.994 | 0.948 |
| 10m without buildings | 0.995 | 0.985 | 0.979 | 0.927 |
| 10m with buildings | 0.995 | 0.985 | 0.987 | 0.975 |
| 20m without buildings | 0.978 | 0.967 | 0.959 | 0.902 |
| 20m with buildings | 0.978 | 0.966 | 0.964 | 0.926 |

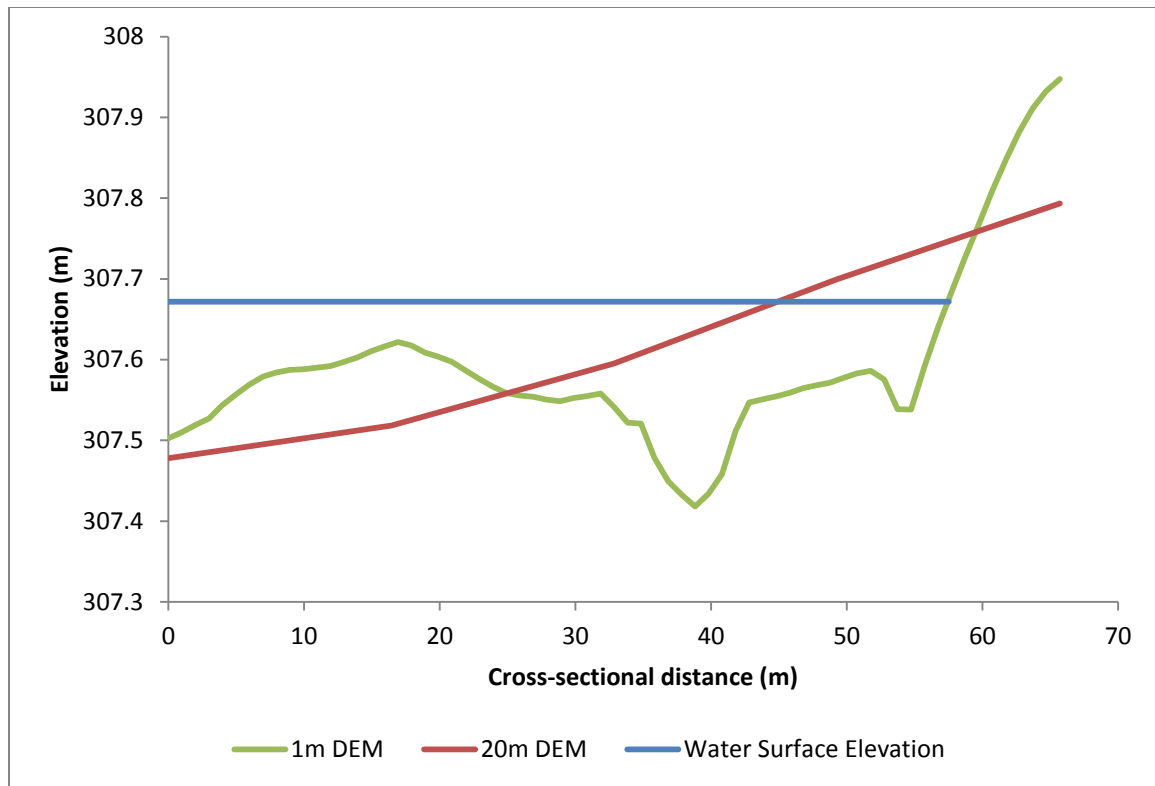


Figure 5.8. Cross-section of topography and water surface elevation.



Figure 5.9. Plan view of cross-section of complex urban topography.

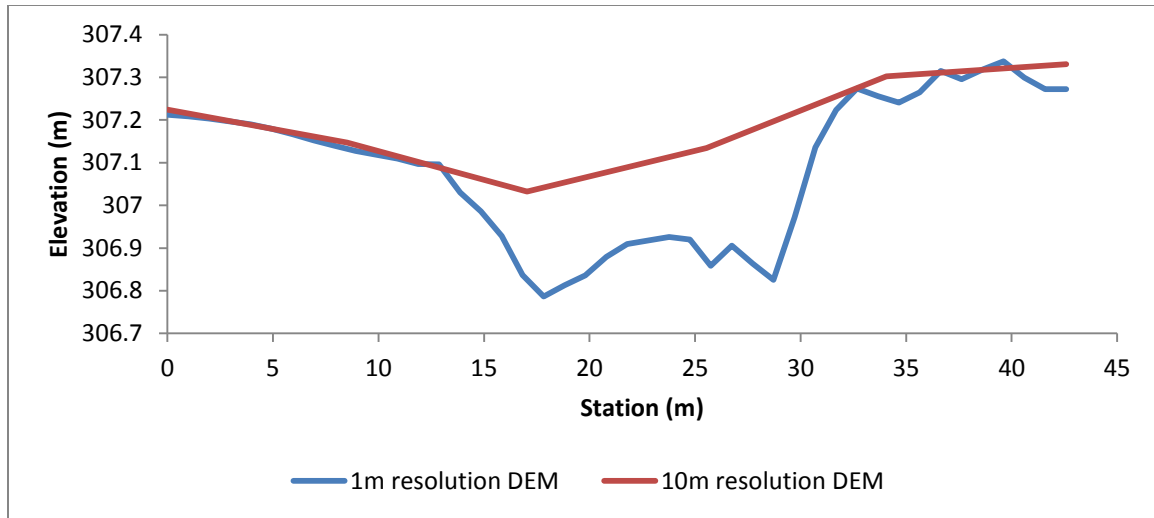


Figure 5.10. Cross-section of complex urban topography showing elevation differences in the location of a street at 1m and 10m resolutions.

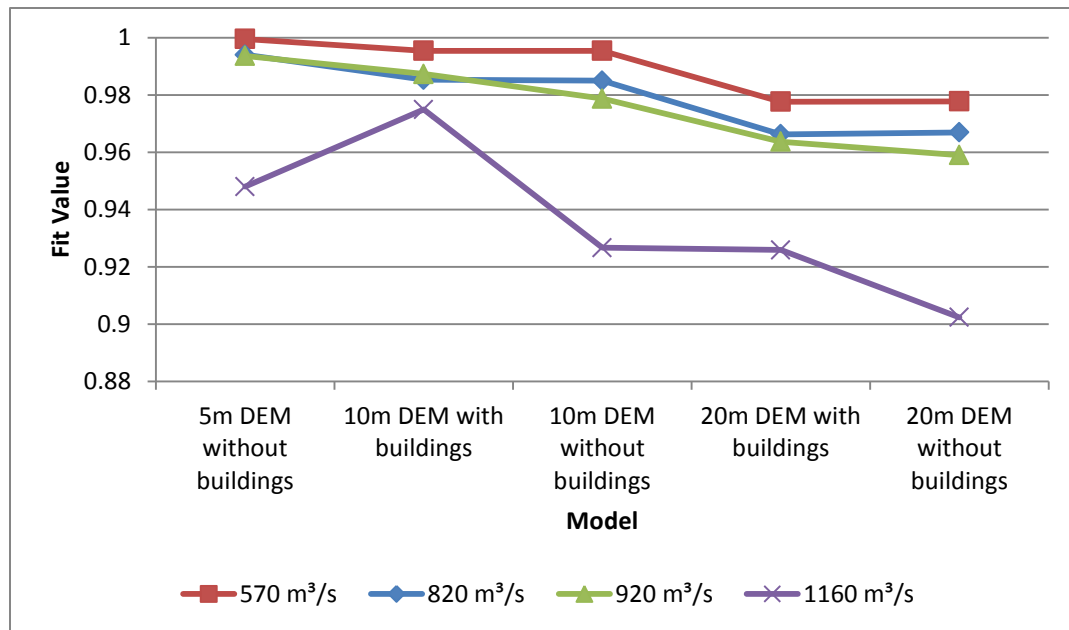


Figure 5.11. Fit values as compared to simulation results from the 5 m model including buildings after re-sampling.

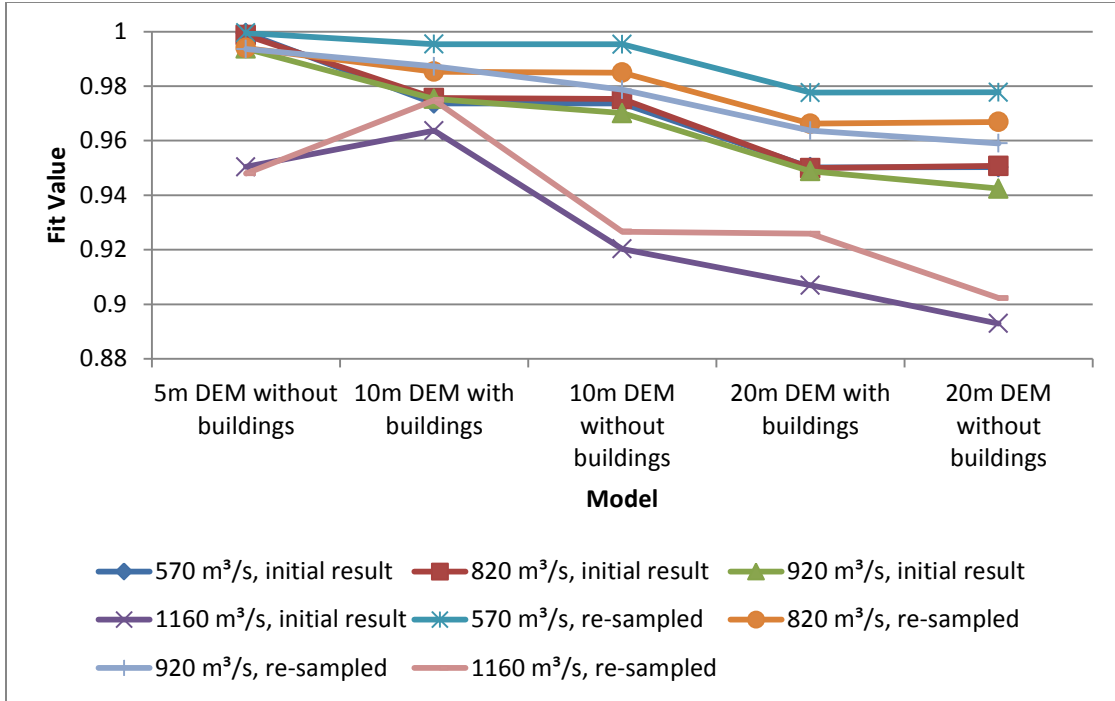


Figure 5.12. Fit values of all simulations compared to 5 m model with buildings included.

Table 5.2. Difference in average depth from the 5 m model with buildings for each other model.

| Discharge | 570 m³/s | 820 m³/s | 920 m³/s | 1160 m³/s |
|-----------------------|----------|----------|----------|-----------|
| 5m without buildings | -0.002 | 0.003 | 0.051 | 0.177 |
| 10m without buildings | 0.008 | 0.101 | 0.145 | 0.273 |
| 10m with buildings | 0.008 | 0.092 | 0.096 | 0.091 |
| 20m without buildings | 0.081 | 0.064 | 0.371 | 0.411 |
| 20m with buildings | 0.08 | 0.016 | 0.327 | 0.288 |

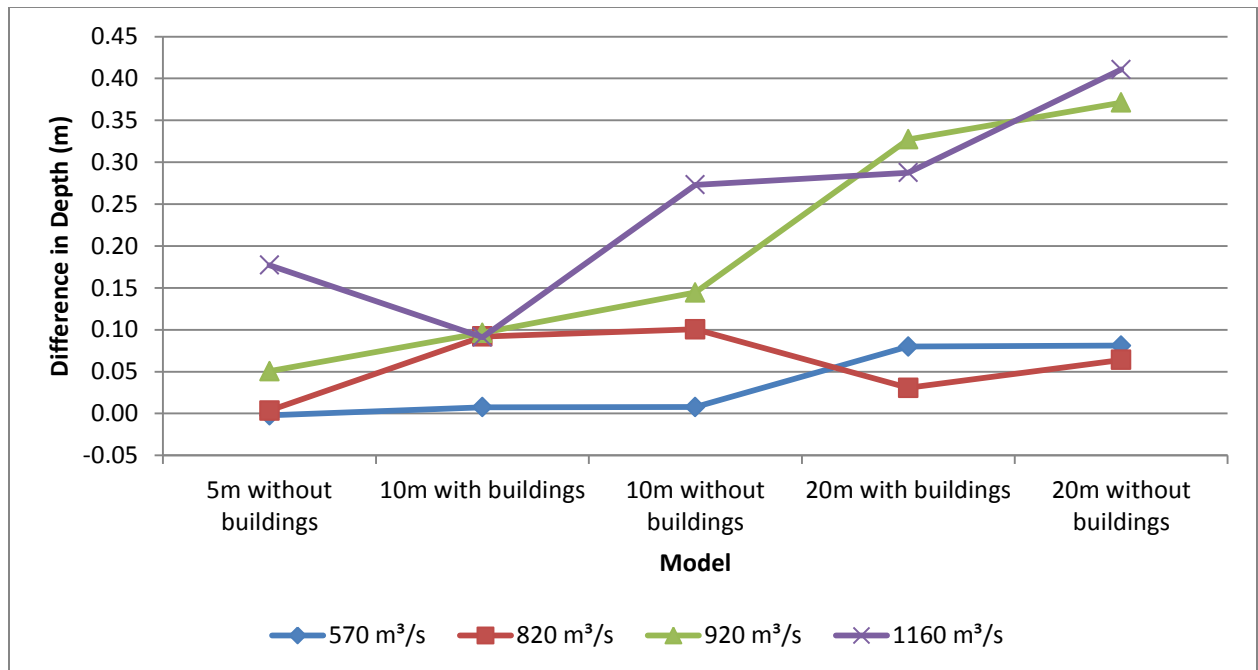


Figure 5.13. Difference in average depth from the 5 m model with buildings for each other model.

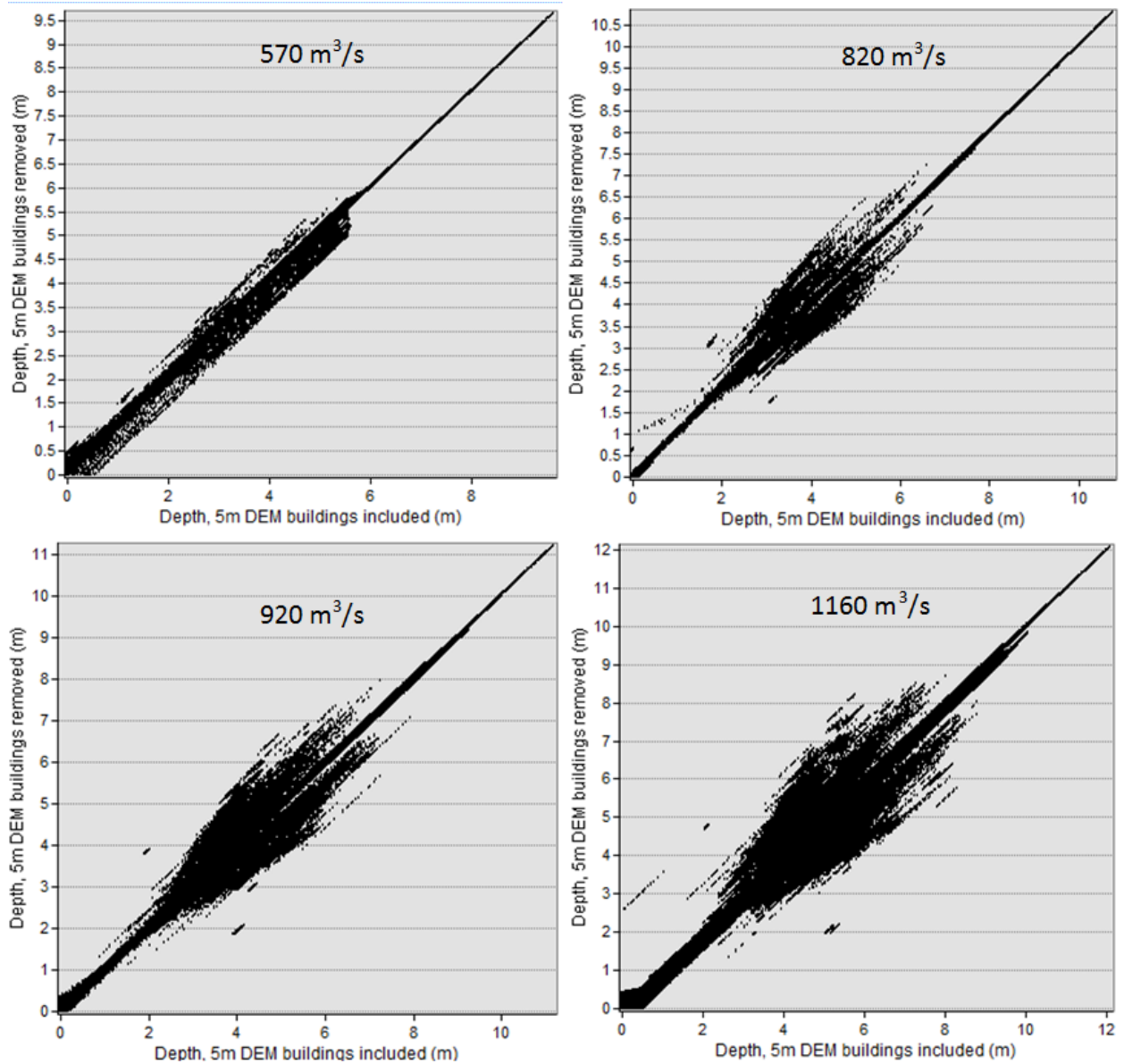


Figure 5.14. Scatter plot of depth comparing the 5 m model without buildings to the 5 m model with buildings.

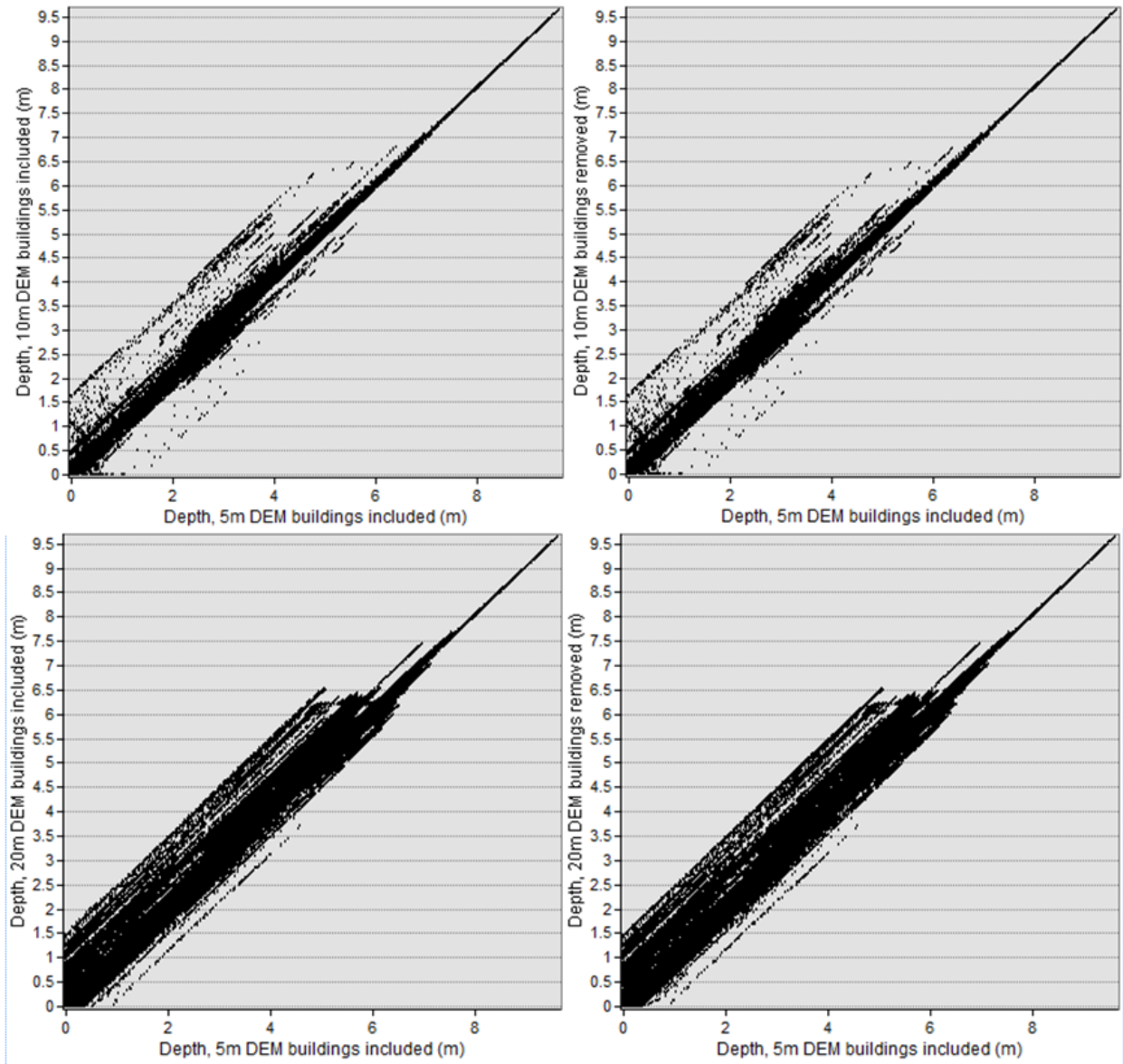


Figure 5.15. Scatter plot of depth comparing results from the 10 and 20 m models both with and without buildings at a discharge of $570 \text{ m}^3/\text{s}$.

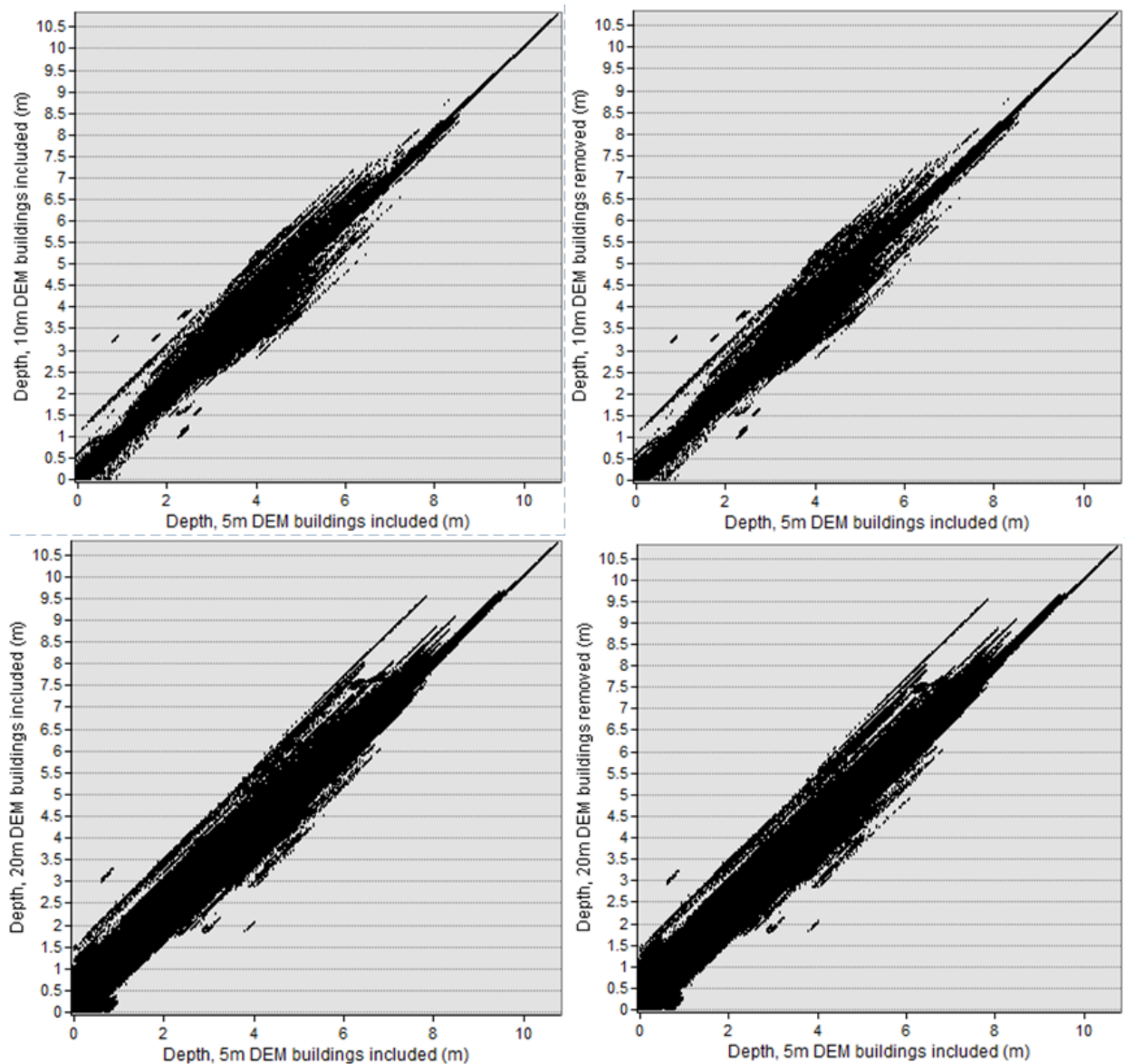


Figure 5.16. Scatter plot of depth comparing results from the 10 and 20 m models both with and without buildings at a discharge of $820 \text{ m}^3/\text{s}$.

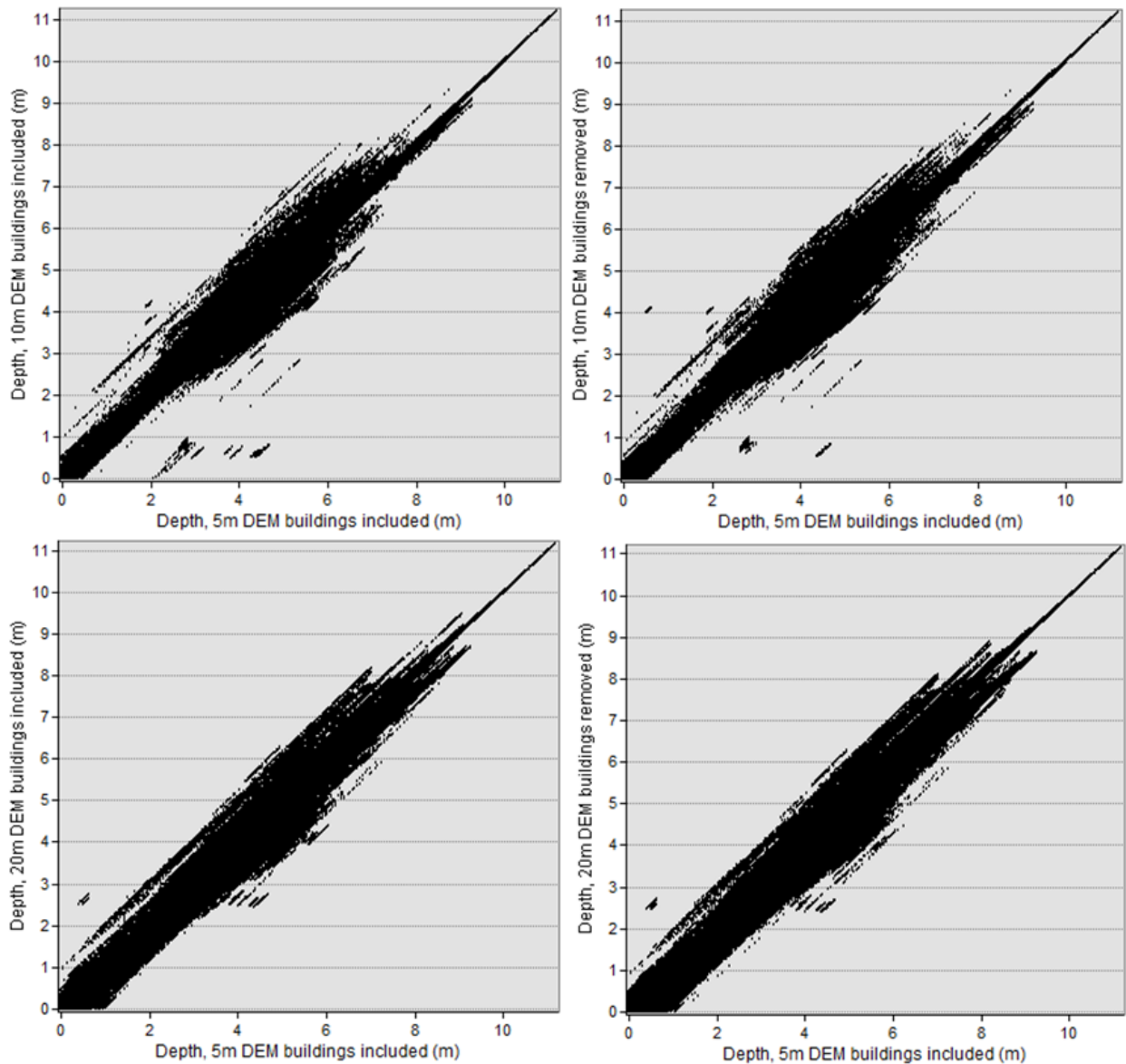


Figure 5.17. Scatter plot of depth comparing results from the 10 and 20 m models both with and without buildings at a discharge of $920 \text{ m}^3/\text{s}$.

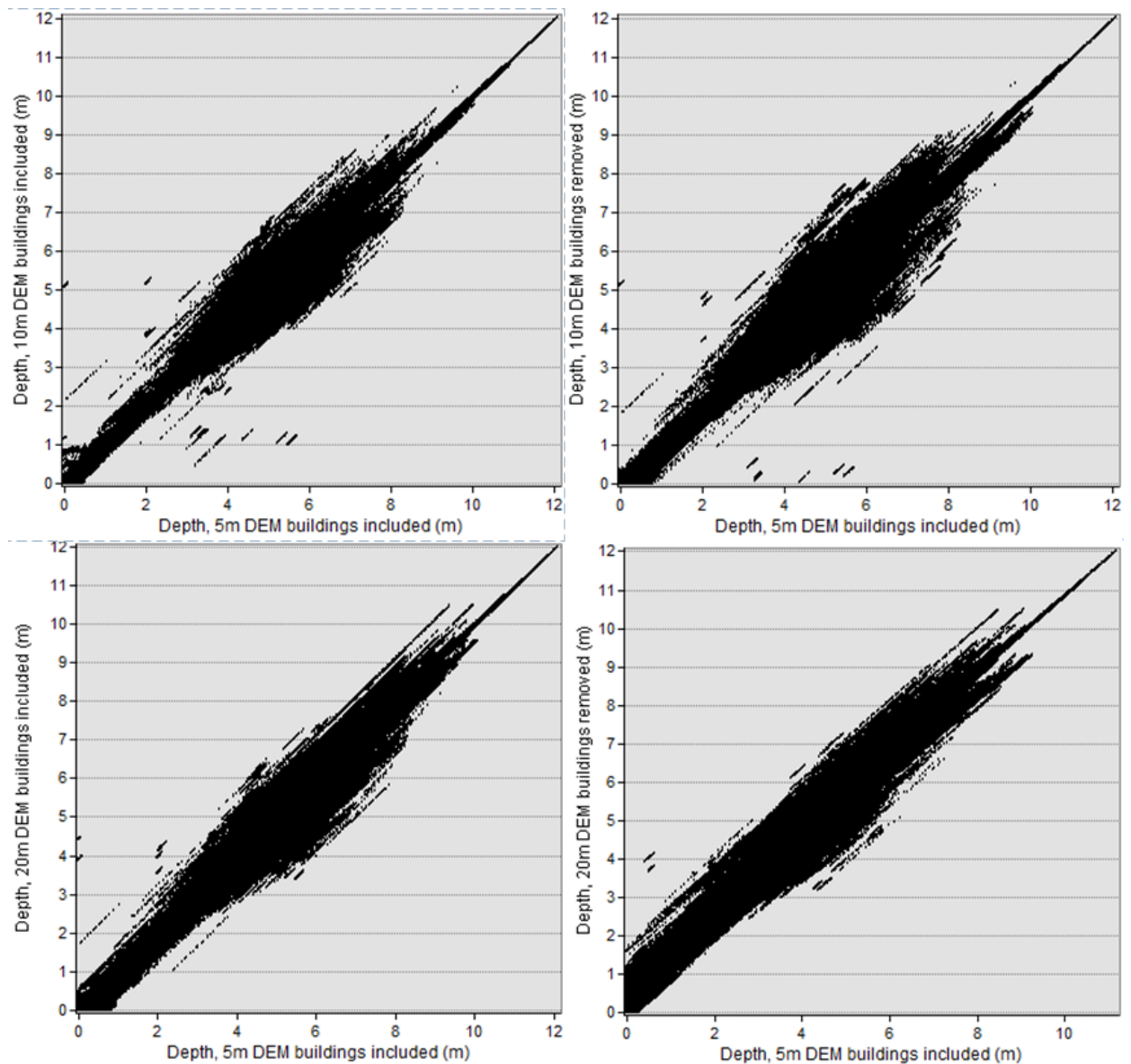


Figure 5.18. Scatter plot of depth comparing results from the 10 and 20 m models both with and without buildings at a discharge of $1160 \text{ m}^3/\text{s}$.

Table 5.3. Computation times for each 3 day simulation in hours. Simulations were performed using dual six-core 2.67 GHz Xeon processors with 12 GB of RAM.

| | 1952800 comp. cells, time step = 0.6 s | | 488150 comp. cells, time step = 1.2 s | | 122576 comp. cells, time step = 2 s | |
|------------------------|---|-------------------------|--|--------------------------|--|--------------------------|
| | 5m with buildings | 5m without buildings | 10m with buildings | 10m without buildings | 20m with buildings | 20m without buildings |
| 570 m ³ /s | 70.09 | 72.50 | 5.97 | 5.98 | 0.59 | 0.78 |
| 820 m ³ /s | 78.20 | 75.92 | 6.87 | 6.88 | 0.91 | 0.84 |
| 920 m ³ /s | 78.99 | 77.27 | 8.46 | 8.12 | 0.78 | 0.83 |
| 1160 m ³ /s | 83.22 | 82.62 | 8.42 | 7.99 | 1.01 | 0.96 |

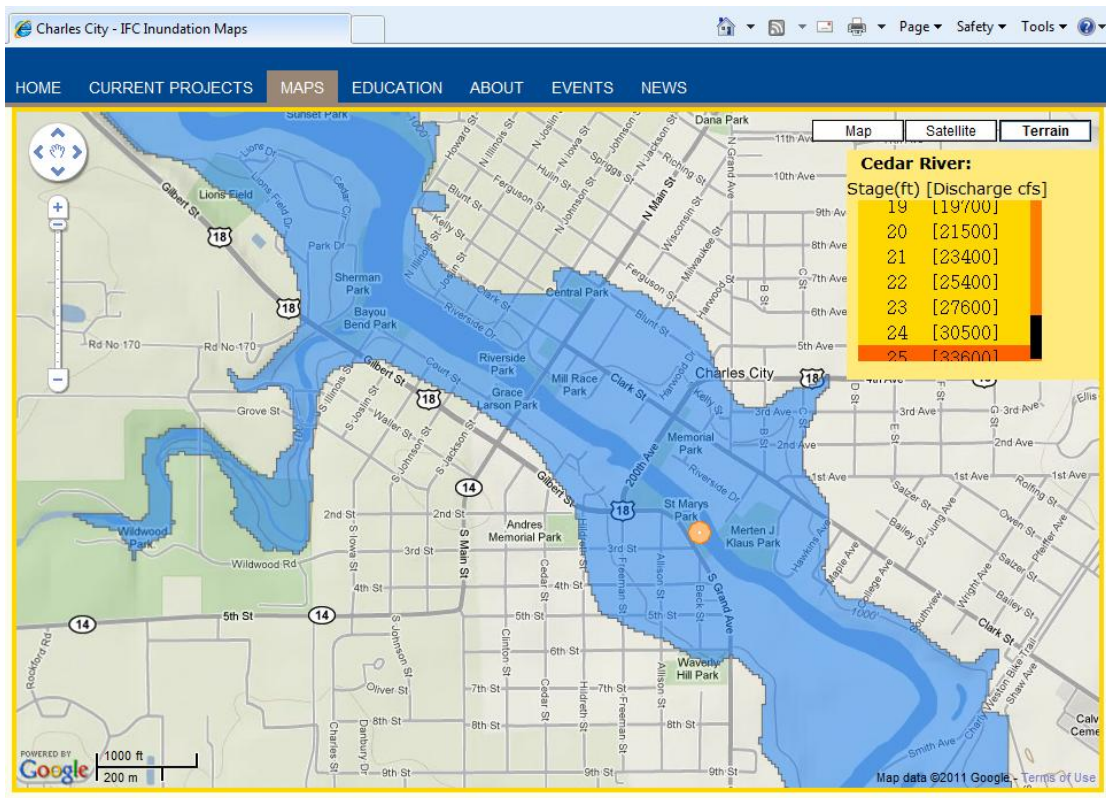


Figure 5.19. An example of the Iowa Flood Center user interface. Users can select inundation area by predicted stage to make decisions about possible risk.

CHAPTER 6: SUMMARY AND RECOMMENDATIONS

6.1 Summary

This study presents the development of a high-resolution 1D/2D coupled flood model of Charles City, Iowa. The Navier-Stokes equations can be applied three-dimensionally; however, in most cases it is unnecessary to incorporate such complexity into flood simulations. Simplified forms of the Navier-Stokes and continuity equations, known as the St. Venant equations, are used as the governing equations for a hydrodynamic simulation.

The simulations developed in this study used a coupled 1D/2D MIKE FLOOD model, where flow in the stream channel is modeled one-dimensionally and flow over the floodplain is modeled two-dimensionally. Coupling the 1D and 2D models maximizes the benefits of both models. Modeling the stream channel one-dimensionally provides a better representation of flow through structures and allows for lower mesh resolution in the 2D model, decreasing computational time. Modeling the floodplain two-dimensionally provides a better representation of complex topography than a 1D model, especially in urban settings.

The model was created by incorporating channel bathymetry into LiDAR topography. Structure geometry was modeled one-dimensionally. The 2001 National Land Cover Dataset was used to determine land cover. Manning's "n" roughness parameters were assigned according to land use and existing literature. Measured water surface elevations were used to calibrate the upstream portion of the model and a USGS stream gage rating curve was used to calibrate the downstream portion of the model. Analyses were performed to determine the model's sensitivity to changes in eddy viscosity, channel roughness, surface roughness in the floodplain. The model was found to be relatively insensitive to changes in eddy viscosity and surface roughness in the floodplain. The model was very sensitive to changes in the channel roughness. An

additional sensitivity analysis was performed to determine the model's sensitivity to changes in mesh resolution and the effect of removing buildings from the topography. Lowering the mesh resolution resulted in a decreased inundation extent and water surface elevation. Removing buildings from the model also reduced inundation extents, especially at higher flows where the water encroached upon urban areas.

The results from the mesh resolution sensitivity analysis were used to determine the effectiveness of using a re-sampling method to improve results produced by simulations with coarse resolution meshes. The re-sampling method produces high-resolution results from coarse-resolution simulations, significantly reducing computation time. The re-sampling method increases resolution of the results from a model using a coarse mesh, as well as removing disconnected areas and filling gaps in the inundation areas created by buildings. In all cases, the re-sampling method increased inundation area and improved the measurement of fit as compared to results from a high-resolution simulation.

After modifying the geometry to account for planned changes to the stream channel in Charles City, this model was used to create a library of steady flow inundation maps. The maps will be available to the public on the Iowa Flood Center website. These maps can be used by residents and decision makers in Charles City to determine potential risk from forecasted flood stages.

6.2 Future Work

A number of assumptions were used to simplify the development of the model used in this study. Storm sewers and tributaries to the Cedar River were neglected. Additional inflow from tributaries may affect model results. Incorporating storm sewers into the simulations and tributaries will also improve the physical consistency of the model.

Very little data were available for model calibration. Additionally, inclusion of planned changes to the stream channel reduced the reliability of the calibration parameters. A Bayesian type probabilistic investigation of model uncertainty as suggested by Bates (2004) may be used to determine model parameters. Due to time constraints, a probabilistic investigation of model uncertainty was not feasible. The model used in this study was created using the 2009 release of MIKE FLOOD, which does not support parallel processing. Parallel processing has been introduced to MIKE FLOOD in the most recent 2011 release. With the improvement in computation time through parallel processing, a Monte Carlo type analysis of model uncertainty should be feasible. Decreased computation times from parallel processing, combined with using the re-sampling tool investigated in this study, may also provide the potential for real-time flood forecasting with a coarse resolution model.

BIBLIOGRAPHY

- Aronica, G., B. Hankin, and K. Beven. "Uncertainty and equifinality in calibrating distributed roughness coefficients in a flood propagation model with limited data." *Advances in Water Resources*, 1998: 349-365
- Bates, P.D., and A.P.J. De Roo. "A simple raster-based model for flood inundation modeling." *Journal of Hydrology*, 2000: 54-77
- Bates, P. D., M. S. Horritt, G. Aronica, and K. Beven. "Bayesian updating of flood inundation likelihoods conditioned on flood extent data." *Hydrological Processes*, 2004: 3347-3370
- Bishop, W.A., and C.L. Catalano. "Benefits of Two-Dimensional Modelling for Urban Flood Projects" *Conference on Hydraulics in Civil Engineering*, 2001: 47-54
- Calenda, G.C., C.P. Mancini, and E. Volpi. "Distribution of Extreme Peak Floods of the Tiber River from the XV Century." *Advances in Water Resources*, 2005: 615-625.
- Chow, V. T. *Open-Channel Hydraulics*. New York: McGraw-Hill, 1959.
- Cook, A., and V. Merwade. "Effect of topographic data, geometric configuration, and modeling approach on flood inundation mapping." *Journal of Hydrology*, 2009: 131-142
- Daluz Vieira, J.H. "Conditions Governing the Use of Approximations for the Saint-Venant Equations for Shallow Surface Water Flow." *Journal of Hydrology*, 1983: 43-58
- DHI. MIKE 11 Reference Manual. MIKE by DHI, 2009.
- DHI. MIKE 21 Flow Model: Hydrodynamic Module Scientific Documentation. MIKE by DHI, 2009.
- DHI. MIKE FLOOD: 1D-2D Modelling User Manual. MIKE by DHI, 2009
- Dhondia, J.F., and G.S. Stelling. "Application of One Dimensional-Two Dimensional Integrated Hydraulic Model for Flood Simulation and Damage Assessment." *Hydroinformatics*, 2002:1-12
- Domeneghetti, A., A. Castellarin, A. Brath. "Effects of Rating-Curve Uncertainty on the Calibration of Numerical Hydraulic Models." *First IAHR European Congress*, 2010
- Eash, D.A. "Techniques for Estimating Flood-Frequency Discharge for Streams in Iowa." U.S. Geological Survey, Water-Resources Investigations Report 00-4233, 2001
- Fewtrell, T.J., P.D. Bates, M. Horritt, and N.M. Hunter. "Evaluating the effect of scale in flood inundation modeling in urban environments." *Hydrological Processes*, 2008: 5107-5118

- Frank, E.A., A. Ostan, M. Coccato, and G.S. Stelling. "Use of an integrated one-dimensional/two-dimensional hydraulic modeling approach for flood hazard and risk mapping." In *River Basin Management*, by R.A. Falconer and W.R. Blain, 99-108. Southampton, UK: WIT Press, 2001
- Gilles, Daniel W. *Application of Numerical Models For Improvement of Flood Preparedness*. MS Thesis, The University of Iowa, 2010.
- Hall, J.W., S Tarantola, P.D. Bates, and M.S. Horritt. "Distributed Sensitivity Analysis of Flood Inundation Model Calibration." *Journal of Hydraulic Engineering*, 2005: 117-126
- Horritt, M.S., and P.D. Bates. "Effects of spatial resolution on a raster based model of flood flow." *Journal of Hydrology*, 2001: 239-249
- Horritt, M.S. and P.D. Bates. "Evaluation of 1D and 2D numerical models for predicting river flood inundation." *Journal of Hydrology*, 2002: 87-99
- Lin, B., J.M. Wicks, R.A. Falconer, and K. Adams. "Integrating 1D and 2D hydrodynamic models for flood simulation." *Proceedings of the ICE – Water Management*, 2005: 19-25
- Merwade, V., A. Cook, and J. Coonrod. "GIS techniques for creating river terrain models for hydrodynamic modeling and flood inundation mapping." *Environmental Modelling & Software*, 2008: 1300-1311
- Pappenberger, F., K. Beven, M. Horritt, and S. Blazkova. "Uncertainty in the calibration of effective roughness parameters in HEC-RAS using inundation and downstream level observations." *Journal of Hydrology*, 2005: 46-69
- Pappenberger, F.P., P. Matgen, K.J. Beven, H. Jean-Baptiste, L. Pfister, and P. Fraimont de. "Influence of uncertain boundary conditions and model structure on flood inundation predictions." *Advances in Water Resources*, 2006: 1430-1449
- Pappenberger, F, K. Beven, K. Frodsham, R. Romanowicz, P. Matgen. "Grasping the unavoidable subjectivity in calibration of flood inundation models: A vulnerability weighted approach." *Journal of Hydrology*, 2007: 275-287
- Patro, S., C. Chatterjee, S. Mohanty, R. Singh, and N. S. Ragwanshi. "Flood Inundation Modeling using MIKE FLOOD and Remote Sensing Data." *Journal of the Indian Society of Remote Sensing*, 2009: 107-118
- Piotrowski, Jesse A. *Development of a High-Resolution Two-Dimensional Urban/Rural Flood Simulation*. MS Thesis, The University of Iowa, 2010.
- Romanowicz, R. and K. Beven. "Estimation of flood inundation probabilities as conditioned on event inundation maps." *Water Resour. Res.*, 39(3), 1073, 2003
- Samuels, P.G. "Cross section location in one-dimensional models." *International Conference on River Flood Hydraulics*, 1990: 339-350
- Sauer, V.B., and R.W. Meyer, *Determination of Error in Individual Discharge Measurements*. Open-File Report, Norcross, Georgia: U.S. Geological Survey, 1992.

- Stelling, G.S., and A. Verwey. "Numerical Flood Simulation" *Encyclopedia of Hydrological Sciences*, 2006.
- Syme, W.J., M.G. Pinnell, and J.M. Wicks. "Modelling Flood Inundation of Urban Area in the UK Using 2D / 1D Hydraulic Models." *Proceedings of the 8th National Conference on Hydraulics in Water Engineering*, The Institution of Engineers, Australia, 2004
- Verwey, A. "Latest Development in Floodplain Modelling – 1D/2D Integration." *Conference on Hydraulics in Civil Engineering*, 2001